

Design Rules for Phase-Change Materials in Data Storage Applications

Dominic Lencer, Martin Salinga, and Matthias Wuttig*

Phase-change materials can rapidly and reversibly be switched between an amorphous and a crystalline phase. Since both phases are characterized by very different optical and electrical properties, these materials can be employed for rewritable optical and electrical data storage. Hence, there are considerable efforts to identify suitable materials, and to optimize them with respect to specific applications. Design rules that can explain why the materials identified so far enable phase-change based devices would hence be very beneficial. This article describes materials that have been successfully employed and discusses common features regarding both typical structures and bonding mechanisms. It is shown that typical structural motifs and electronic properties can be found in the crystalline state that are indicative for resonant bonding, from which the employed contrast originates. The occurrence of resonance is linked to the composition, thus providing a design rule for phase-change materials. This understanding helps to unravel characteristic properties such as electrical and thermal conductivity which are discussed in the subsequent section. Then, turning to the transition kinetics between the phases, the current understanding and modeling of the processes of amorphization and crystallization are discussed. Finally, present approaches for improved high-capacity optical discs and fast non-volatile electrical memories, that hold the potential to succeed present-day's Flash memory, are presented.

1. Introduction and Basics

Throughout the history of mankind, the ability to store, share, develop, rearrange and combine information has been key to its evolution. We may only guess what course history would have taken if apparently simple inventions such as pen, paper and letterpress, but also the modern wonder of computers would not be omnipresent, but existed only in the minds of gifted science-fiction writers. Thus, there might be only few fields of research that have an equally important impact on the fate of mankind

as those of data storage and processing. We may hence only approach the limits of our cultural advancement if we succeed in providing memories that combine availability with speed and reliability.

A particularly promising approach for such data storage devices is based on the fast reversible switching of so-called phase-change materials between an amorphous and a crystalline state. Both phases are characterized by very different material properties, thus providing the contrast required to distinguish between logical states. Phase-change recording was initiated in the 1960s by Ovshinsky.^[1] It is the state-of-the-art technique for rewritable optical storage since the market introduction of the CD-RW in 1996, and continues to hold this position up to now in the form of the rewritable incarnation of the Blu-ray disc format (i.e., BD-RE). It is also among the most promising candidates to succeed Flash memory, with the potential to fulfill its duties at a speed currently reached by the volatile DRAM. However, phase-change memories are far from being just an engineering issue. A wide scope of

aspects in material science is involved in understanding phase-change materials, founding the scientific interest in these materials that has led to hundreds of publications. Ultimately, an in-depth understanding of the few known successful phase-change materials is commonly thought to lead to design rules for optimal materials, which is one of the driving forces of the field. It is the aim of this article to provide an overview over the current state of understanding of phase-change materials that has greatly improved within the last few years.

To start, a brief introduction into the basics of phase-change recording shall be given. The principle of operation is illustrated in **Figure 1**. A small portion of a phase-change material is switched between the crystalline and amorphous state by providing a precisely controlled amount of heat. Currently, either laser pulses or electrical pulses are employed as heat sources depending on the application in optical or electronic data storage. Starting from a crystalline bit, the temperature needs to be first elevated above the liquidus temperature T_l using a short, high intensity (high current) pulse. Since only a spatially confined region is heated up, a huge temperature gradient between the molten bit and the surrounding material is obtained, leading to high cooling rates of about 10^{10} K/s. If the melt cools fast

Dr. D. Lencer, Dr. M. Salinga, Prof. M. Wuttig
I. Physikalisches Institut IA
RWTH Aachen University
52056 Aachen, Germany
E-mail: wuttig@physik.rwth-aachen.de

Prof. M. Wuttig
Jülich-Aachen Research Alliance
Section Fundamentals of Future Information Technology (JARA-FIT)
52056 Aachen, Germany

DOI: 10.1002/adma.201004255

enough, crystallization is bypassed. Instead a melt-quenched amorphous bit is formed if the temperature falls fast enough below a critical temperature, the glass transition temperature T_g . In this low temperature regime, the atomic mobility is so small that crystallization, though energetically favorable, is kinetically hindered. To switch from the amorphous back to the crystalline state, the temperature of the bit needs to be elevated for a sufficiently long time to a temperature where the atomic mobilities are high enough for crystallization to occur. Hence, the sample has to be heated significantly above the glass transition temperature. To read out whether a bit is amorphous or crystalline, low intensity (low current) pulses are employed to distinguish between low and high reflectivity (conductivity).

Noteworthy are the timescales of phase changes. Typically, crystallization is the slowest process involved. Nevertheless, under optimal conditions it may proceed in a matter of nanoseconds at elevated temperatures. At ambient conditions, however, crystallization of an amorphous bit must not take place within many years to ensure data retention. This means that the crystallization rate of phase-change materials must increase by up to twenty orders of magnitude while the temperature is increased by only a few hundred Kelvin. Thus, an in-depth understanding of the crystallization kinetics is required to find out where this significant temperature-dependence stems from and how it can be controlled.

The task to be accomplished for material researchers is to find out which materials are suitable for application. This is a challenging quest, since the requirements regarding kinetics are not the only ones phase-change materials have to meet. These requirements for storage applications are listed in **Table 1**.

In order to distinguish between the phases, reflectivity and conductivity must differ significantly. At first sight, this seems to require also a significant difference in local structure. But then the question arises, why the phase transition is so fast. The understanding of this apparent conflict has made significant progress in the recent past and is addressed in the following sections. Further requirements may occur in the context of a particular type of application. For instance, a small density contrast may be desirable to improve the cyclability of a memory cell. At the same time, a small density contrast could possibly be accompanied by a small property contrast which would hamper the read-out of stored data. This demonstrates that optimal phase-change materials must provide a compromise of numerous, sometimes conflicting demands. In the past, a number of materials have been identified which meet these requirements. Since these materials have often been found by an empirical approach, it is not clear whether these materials are really best suited to meet the demands listed in **Table 1**.

Most of the families of phase-change materials already identified can be found in the ternary Ge:Sb:Te-phase diagram shown in **Figure 2**. The most prominent materials such as $\text{Ge}_2\text{Sb}_2\text{Te}_5$ are located on the pseudo-binary line connecting GeTe and Sb_2Te_3 .^[3,4] Besides Sb_2Te_3 , also Sb_2Te offers suitable properties when combined with silver and indium, yielding the widely employed AgInSbTe (abbrev. AIST).^[5] Finally, another material family that has attracted considerable interest in the last years is found here, namely modifications of antimony such as $\text{Ge}_{15}\text{Sb}_{85}$.^[6,7] It stands out due to the fact that it does not contain a chalcogenide component, but can be understood in terms of



Dr. Dominic Lencer studied physics at RWTH Aachen University and received his diploma in September 2006. His thesis was conducted both at the Institute of Physics (IA) of RWTH Aachen University as well as in the Department of Engineering and Applied Sciences at Harvard University, advised by Professor Matthias Wuttig and Professor Frans Spaepen. He was concerned with crystallization kinetics and ab initio modeling of phase-change materials. Since October 2006, he continued his research in Aachen, and obtained his doctoral degree in December 2010.



Dr. Martin Salinga is a staff member at RWTH Aachen University, Germany. He obtained his diploma in 2004 and his Ph.D. degree in 2008, both in physics, from RWTH Aachen. For his diploma thesis on the crystallization kinetics of phase-change materials used in optical data storage, he performed his research both at RWTH Aachen and at Harvard University. From February 2005 until September 2006, he was on assignment at the IBM Almaden Research Center, investigating both crystallization kinetics and electronic properties of phase-change materials. Back at RWTH Aachen, Dr. Salinga continues his studies on phase-change materials while also teaching.



Matthias Wuttig is a Full Professor of Physics at the University of Technology, Aachen, Germany since 1997 and JARA-Professor at Research Center Jülich. He is speaker of the strategy board (since 2009) and was Dean of the Faculty of Science, Mathematics and Computer Sciences (2006-2008). He leads the Research Group: Physics of Novel Materials, which characterizes and investigates novel materials with unique optical and electronic properties. Recently this research has been focused on the explanation of the unique property portfolio of phase-change materials.

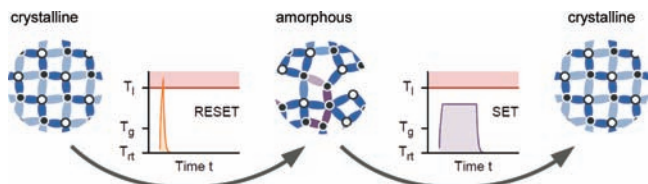


Figure 1. The operation principle of phase-change devices is based on the reversible switching between the crystalline and amorphous state. Amorphization (also called *RESET*-operation) of a bit proceeds via melt-quenching, employing short current pulses as heat sources. In optical recording, short laser pulses are utilized instead. The resulting huge temperature difference between the confined melt and the surrounding material leads to extremely high cooling rates. Thus, the disorder of the liquid is frozen in. Crystallization (*SET*-operation) requires annealing of an amorphous bit at a temperature below the melting temperature for the atoms to adopt the energetically favorable crystalline order. Reproduced from Ref. [2].

doped antimony. Doping in the field of phase-change materials refers to much larger concentrations (typically on the order of some percent) than in usual semiconductors such as silicon. We will tackle the role of stoichiometry in more detail later on, but here it should be mentioned that $\text{Ge}_{15}\text{Sb}_{85}$ also is close to the eutectic composition, whereas all other materials mentioned before are single-phase materials. The search for eutectics was one of the first rules for the empirical identification of phase-change materials. Eutectics are characterized by two supposedly attractive properties; their low liquidus temperature reduces the power consumption necessary to melt the material. In addition, eutectics are easy to amorphize since typically the glass transition temperature varies much less with composition than the liquidus temperature does. Hence, materials that are easy to amorphize may thus be obtained by reducing the temperature interval that has to be bypassed by quenching. Thus, this feature facilitates the formation of an amorphous bit upon melt-quenching by circumventing rapid crystallization. Furthermore, an eutectic material melts congruently, but it does not form a homogeneous phase upon crystallization, at least not in equilibrium. Given the required temperature and time, decomposition is inevitable, posing challenges for the stability and cyclability of a phase-change device.^[8,9] Ultimately, that was the reason why research shifted from eutectics to single-phase materials for optical applications. This example once again

demonstrates how conflicting the requirements phase-change materials have to meet can be.

These discussions immediately raise the question why the materials in the ternary Ge:Sb:Te-phase diagram work as phase-change materials, and whether materials, that are composed of other elements, would work as well, or even better. While this question can in part be tackled by empirical search algorithms, a microscopic understanding could provide a superior route to material optimization. This might help to understand how both the switching speed and the property contrast can be optimized simultaneously by stoichiometry variation. How can this goal be reached?

If you want to understand function, you have to study structure. This famous expression by Sir Francis Crick (thanks to Professor R. Jones for bringing this quotation to our attention) serves as the guideline for the first half of this review paper. Presumably, the significant difference in optical reflectivity and electrical conductivity between the amorphous and the crystalline state is related to substantial differences in the atomic arrangement. Hence, we will first review the structures of crystalline phase-change materials, and subsequently relate them to the bonding. The comparison to the structure and bonding in the amorphous phase will then allow us to identify the origin of the contrast that these materials exhibit. Understanding structure and bonding then provides an efficient framework to discuss other physical properties that are relevant for the materials

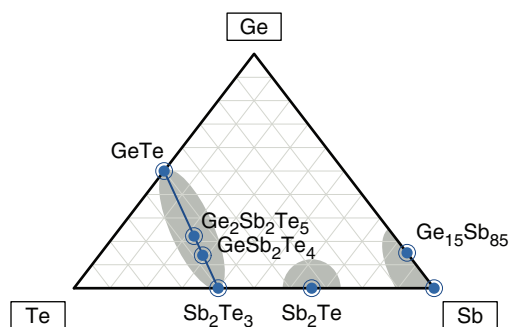


Figure 2. Most phase-change materials are found within the ternary Ge:Sb:Te-phase diagram. In particular, the pseudo-binary line between GeTe and Sb_2Te_3 stands out as it hosts the most prominent phase-change materials composed as $(\text{GeTe})_m(\text{Sb}_2\text{Te}_3)_n$, with m and n being integer numbers. Reproduced from ref. [2].

Table 1. Numerous material requirements for phase-change materials follow from the desired use in data storage applications. This table compiles the most important demands. The task material research is confronted with is to find optimal materials that suit these needs.

Application Requirement	Material Requirement
Distinguishable logical states	ability to switch between phases that exhibit significantly different optical/electrical properties
Fast data transfer rates	rapid crystallization at elevated temperatures
Stability	no crystallization at ambient temperatures
Scalability/Data density	simple compositions, insensitivity to composition variations, functionality retained in small volumes with large interfaces
Cyclability	no irreversible modifications due to the switching process itself (e.g., electromigration), intrinsic change of the material over time (e.g., relaxation) or interaction with the environment (e.g., chemical reaction with the electrodes)
Operation of PCRAM at low voltages	nonlinear electrical behavior in the amorphous state and reasonably high resistivity in the crystalline state
Easy to fabricate	production compatible with established semiconductor manufacturing processes and compliant with environmental legislation

and their prospective applications. Finally, both the processes of amorphization and crystallization are reviewed, before we conclude with an overview of present and future applications of phase-change materials.

2. Structure and Bonding in the Crystalline and the Amorphous Phase

This chapter will start with a discussion of the atomic arrangement in crystalline phase-change materials. It will be demonstrated that these materials are characterized by a few typical structural motifs, which can be linked to a unique bonding mechanism which prevails in the crystalline phase. Hence, the precise characterization of the atomic arrangement of the crystalline state can provide valuable insight into the bonding of these materials and the resulting properties.

The determination of the structure should be much easier for the crystalline phase than for both the liquid and the amorphous state. The long range order of the crystalline phase enables us to employ the tools of crystallography, with which the precise determination of atomic arrangements is routinely feasible even for crystalline materials having large unit cells and containing several different atomic species. Hence, it appears surprising that even today there are important new discoveries as well as open questions regarding the atomic arrangement of crystalline phase-change materials. Therefore, we will first briefly summarize the challenges to determine the structure of crystalline phase-change materials. As already mentioned in the introduction, one of the attractive properties of phase-change materials is their ability to crystallize on time scales of just a few nanoseconds at elevated temperatures. The underlying reasons for the fast crystallization behavior will be described in the section on transformation kinetics, Section 4. The specific crystallization characteristics of phase-change materials lead to the fact that their crystalline state usually consists of rather small (few tens of nanometers) grains. Usually, these grains form a polycrystalline state without any preferred orientation. This is a serious complication for diffraction tools which are ideally suited for single crystals.

Therefore in recent years it has been attempted to produce single crystalline samples of phase-change materials in the Ge:Sb:Te-system.^[10] These studies have provided new insights into the atomic arrangement of the constituting elemental species. To produce single crystals it is usually unavoidable to work close to thermal equilibrium, while in phase-change recording the corresponding crystallization process typically occurs very far from thermal equilibrium. Hence, the question needs to be addressed if the atomic arrangement in crystalline phase-change materials prepared under conditions close to thermal equilibrium resembles the structural motifs found when crystallization takes place on the timescale of a few nanoseconds. Often the relevant question in phase-change recording is not, what is the most stable atomic arrangement for a given atom if an infinite amount of time is available to explore phase space. Instead, the atom frequently only has a few nanoseconds to find favorable atomic arrangements in the adjacent phase space. Therefore, very often the resulting crystalline phases are metastable, and retain similarities in atomic ordering to the corresponding liquid or amorphous phase they were created from. This is one

important aspect to keep in mind for the remainder of this section. A second promising approach to obtain samples with single crystalline qualities has been pursued as well; epitaxial thin films of Ge₂Sb₂Te₅ grown on GaSb-substrates to overcome the limitations that arise from polycrystalline samples, such as the inability to angularly resolve the Brillouin-zone.^[11] At the same time, the comparability to the properties of typically sputter-deposited thin films needs to be critically reviewed here, too.

Frequently, phase-change materials are deposited by sputtering at room temperature. Under these conditions, the resulting films are usually amorphous. Subsequent heating above the glass transition temperature leads to a polycrystalline film. Hence, the diffraction peaks are rather broad and have a low intensity. This makes the precise determination of atomic positions considerably more difficult. In addition, there is a significant change of atomic volume upon crystallization as can be clearly demonstrated by X-ray reflectometry measurements.^[12] This leads to significant strains upon crystallization,^[13] which also have a profound impact on the position of the diffraction peaks. Finally, there is strong evidence for pronounced anharmonic behavior in the crystalline phase, see Section 3.1. All of these aspects have to be properly taken into account, to obtain the atomic arrangement from the diffraction data of polycrystalline thin film samples.

The occurrence of metastable, polycrystalline phases has important consequences. On the one hand, just as in the case of amorphous samples, the thermal history of a sample affects its properties and has to be carefully considered.^[14,15] On the other hand, this could have very positive consequences as well. Possibly this significantly widens the composition space of suitable phase-change materials. Even materials that are unstable at equilibrium conditions, such as “doped” materials or eutectics, might be suitable for phase-change recording, as long as phase separation or chemical reactions can be suppressed on short timescales. Then, it has to be checked, however, if these detrimental processes have a negative impact on longer time scales, affecting important properties such as cyclability.

2.1. Atomic Structure of the Crystalline Phase

We now turn to the discussion of typical crystal structures of phase-change materials, focusing again on the prototype Ge:Sb:Te-materials. Interesting enough, almost independent of the formation routes chosen, the atomic structures of phase-change materials exhibit generic features and structural motifs, which are quite different from other materials that at first sight should behave similarly. This implies that phase-change materials are characterized by a unique bonding mechanism, which will be discussed in the following section. The two limiting cases of the pseudobinary line, GeTe and Sb₂Te₃, are well suited to discuss the structure and bonding mechanisms that rule phase-change materials, as discussed by Da Silva et al.^[16] (and references therein), see also Figure 3.

2.1.1. The Structure of GeTe

Let us first consider GeTe. It exhibits a structure that closely resembles the rocksalt-structure, with Ge occupying the cation

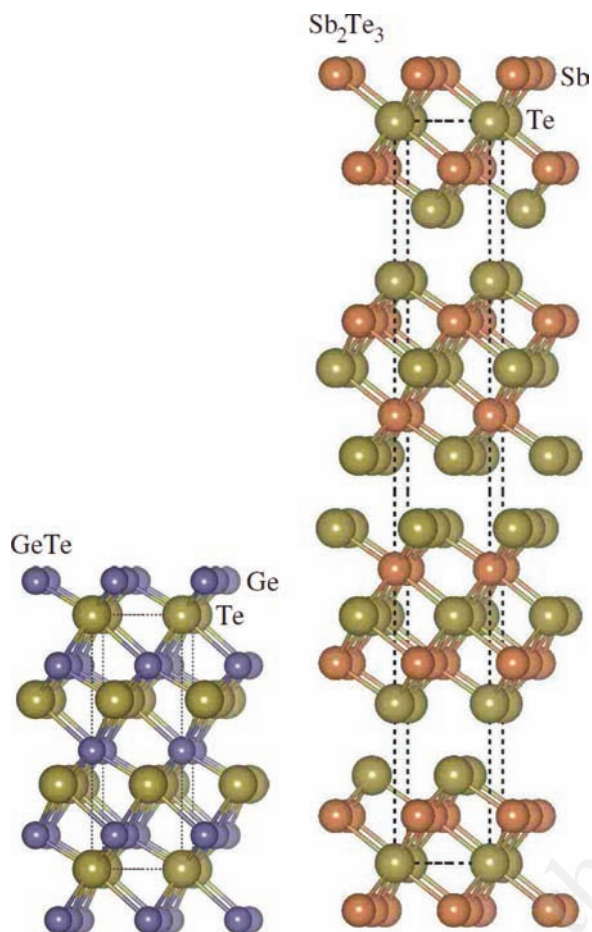


Figure 3. The crystal structures of GeTe and Sb_2Te_3 as explained in the text. Phase-change materials inherit the principal structural features of these two limiting cases. Reproduced with permission from ref. [16]. Copyright 2008, American Physical Society.

and Te the anion sublattice. At temperatures below approximately 700 K, atomic displacements deform this lattice. First, there is a relative shift of the two sublattices along the [111]-direction. This reduces the number of bonds from six to three short bonds (and three long bonds), in line with the Peierls-model of distortions for a system with an average number of three p-electrons.^[17,18] As a secondary effect, the atomic displacements lead to a small decrease of the cell angle. Altogether, a rhombohedral rather than a cubic cell is obtained (Ref. 19 and references therein). Above around 700 K, a second order phase transition lifts the distortion.

2.1.2. The Role of Peierls-Like Distortions

Since these distortions are of utmost importance for phase-change materials, we shall briefly introduce the underlying concept. Though we adopt the common approach to introduce the systematics for a periodic (i.e., crystalline) system, the results on the shifts in the density of states and the local distortions can be transferred to non-crystalline systems as well. As a prerequisite, dominant p-type bonding (equivalent to the absence

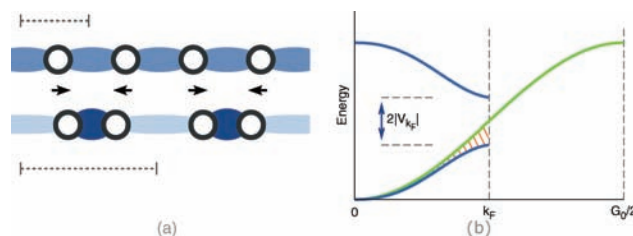


Figure 4. Schematic of a Peierls-distortion for a one-dimensional chain with a half-filled band. By a (periodic) distortion, the size of the Brillouin zone is reduced and a new component of the potential is introduced. This leads to an opening of a gap and concurrently a decrease in energy for the occupied states that is the driving force behind these distortions. Reproduced from ref. [2].

of hybridization between s- and p- states) is assumed, leaving us first with a (hypothetic) highly symmetric six-fold coordination. To simplify matters, we assume a one-dimensional chain of equally spaced atoms with a simple parabolic band structure as shown in **Figure 4**. Depending on the number of electrons or equivalently, the position of the Fermi wavevector k_F , this chain is unstable against a periodic distortion. Given k_F is located within the Brillouin zone,

$$k_F = \gamma \cdot \frac{G}{2}, \quad \gamma < 1 \quad (1)$$

that is a distortion that introduces a Fourier component of the potential at this wavevector, V_{k_F} , leads to the opening of a gap of size $2|V_{k_F}|$ and thus a decrease of the energy of the occupied states. The Brillouin zone shrinks according to the periodicity of the distortion pattern. With this model, we can understand the coordination of GeTe and elemental antimony, for instance, if we assume that each dimension may be treated separately. Then, we have three p-valence electrons per atom out of a maximum of six, one per dimension, which yields $\gamma = 1/2$. Thus, the initially equally long bonds in one dimension split into a short and a long bond. So in three dimensions, three short and three long bonds per atom result. The same line of reasoning can be employed for elemental tellurium, yielding two short and four long bonds per atom and reproducing the experimentally obtained zig-zag chain-structure. However, there is one degree of freedom per dimension, the phase of the distortion that cannot be inferred from the preceding arguments. We note that so far we have not considered additional elastic forces nor the effect of ionicity, that comes into play for non-elemental systems, both counteracting the mechanism of atomic distortions. As mentioned before, Peierls-like distortions can also prevail in non-crystalline systems. The conceptual translation from a periodic to a local picture can be given by local hybridization of the atoms, thus maximizing the degree of saturation of a few short covalent bonds at the expense of less saturated long bonds.

2.1.3. The 8-N-Rule

The above coordination numbers of antimony and tellurium agree with what would have been predicted by the so-called

8-*N*-rule. With *N* being the number of valence electrons of an atom, the rule states that generally, the coordination of an atom in a covalent bonding configuration is equal to 8-*N*. The 8-*N*-rule successfully explains and predicts the atomic coordination in a wide range of materials composed of elements from the groups V, VI and VII.^[17] However, we note that as one goes down in germanium's row of the periodic table, the limits of the 8-*N*-rule become obvious. Elemental lead is not tetrahedrally, but octahedrally coordinated, owing to the fact that due to relativistic effects hybridization becomes unfavorable.^[18] This 8-*N*-rule has to be applied either individually for each atomic species or in a species-averaged manner. An example for the latter behavior is seen in GaAs. On average, this material has 4 valence electrons (As has 5 valence electrons, while Ga has 3). In this case, it can form a tetrahedral atomic arrangement as in the zincblende structure, where every atom has four nearest neighbors and forms a tetrahedral atomic arrangement. In SiO₂, on the contrary, the 8-*N* rule would need to be applied for each atomic species individually; silicon, with its 4 valence electrons, has 4 nearest neighbors of oxygen, while oxygen, with its 6 valence electrons, has 2 nearest neighbors of Si. For GeTe, we see that we need to use an *average* number of five valence electrons per atom. The structures we observe here (and in the following), are remarkably close to six-fold coordination, and the validity of the 8-*N*-rule is only just established by the slight local atomic distortions. This raises the question whether it is reasonable to argue that the 8-*N*-rule is fulfilled, if the difference between nearest- and next-nearest neighbors becomes very small.

2.1.4. The Structure of Sb₂Te₃

Not only the structure of GeTe, but also that of Sb₂Te₃ can be understood in terms of a distorted rocksalt-like structure. Again, there is an atomic alternation as antimony has only tellurium neighbors in an octahedral environment. However, since there is an excess of Te-atoms, these would need to be arranged in neighboring sites. Instead, well separated layers, consisting of a sequence Te-Sb-Te-Sb-Te, form with interlayer bonding between adjacent Te planes being ascribed to Van der Waals-interaction. Their separation can be explained by electrostatic repulsion of the anionic Te-atoms. For the following discussion, it will be instructive to view the space between two layers as occupied by a layer of intrinsic vacancies. The layer periodicity depends on the Sb to Te-ratio as investigated by X-ray diffraction.^[20]

2.1.5. The Structure of Alloys on the Pseudobinary GeTe-Sb₂Te₃ Line

The Ge:Sb:Te-compounds inherit the aforementioned structural ingredients. In the metastable crystalline phase, they exhibit a rocksalt-like structure, with tellurium occupying the anion sublattice. The other, cation sublattice is occupied by germanium, antimony and intrinsic vacancies. Thus, these metastable phases also feature an octahedral-like coordination. The atomic positions show (Peierls-like) distortions from the high-symmetry-positions. For compositions close to GeTe, also a rhombohedral distortion of the unit cell is observed.^[21] Interesting enough, the occupation of the cation sublattice

depends on the thermal history. After crystallization, typically a random, chemically disordered occupation is obtained. Density functional theory calculations have been performed in order to find out whether there is an energetically preferred occupation.^[16,22,23] The principal finding is that certain layer-sequences are favored, with the layers being orientated normal to the [111]-direction. The layer sequence is typically similar to what is found for Sb₂Te₃. The germanium-incorporation leads in most cases to the formation of additional -Te-Ge-Te-sequences within the layer. The initially randomly dispersed vacancies are shifted to form the vacant space in between two layer-stacks. For Ge₁Sb₂Te₄, for instance, Da Silva et al.^[16] obtain a Te-Sb-Te-Ge-Te-Sb-Te-sequence. Though, an intermixing of Ge and Sb seems energetically not very different and has in fact been obtained for Ge₂Sb₂Te₅; here, Ge and Sb atoms do not populate separate but shared layers. It has been argued to arise from a preference of Te-atoms to be surrounded by three Ge and Sb atoms. Without the intermixing, the central Te-layer would be neighbored only by Ge-atoms. We note, however, that the same authors state that the theoretically most favorable structure is likely not obtained by experiment given the mismatch between optical properties calculated for those structures and the measured ones.^[24] Very similar layer-sequences are obtained for the stable, hexagonal phases as shown by Kooi and De Hosson.^[25] Thus, it is reasonable to assume that the disordered metastable phase exhibits a tendency towards the same stacking sequence, but is kinetically hampered by slow atomic diffusion.^[26]

2.1.6. The Role of Intrinsic Vacancies

Considerable attention has been devoted to the investigation of the large concentration of intrinsic vacancies. The formation of a vacancy in a solid corresponds to the creation of a defect which usually requires a large formation energy of several eV. This explains why most semiconductors such as Si, Ge, or GaAs are characterized by very small vacancy concentrations. On the contrary, in a phase-change material such as GeSb₂Te₄, there is a 25% concentration of vacancies on the sublattice otherwise occupied by Ge and Sb. This high intrinsic vacancy concentration is rather unusual. Nevertheless, there are also other semiconductors, such as defective chalcopyrites, which are characterized by a high concentration of intrinsic vacancies. Density functional calculations have been conducted to further investigate the role of intrinsic vacancies. Removing Ge atoms from a randomly occupied cell representing Ge₂Sb₂Te₄ and disposing the Ge atoms in a chemical reservoir of elemental germanium^[27] was shown to lower the energy of the system. The reason for this lowering of the energy is related to the fact that the highest electronic states occupied for Ge₂Sb₂Te₄ are antibonding. Hence, emptying these states by removing Ge atoms lowers the energy of the system. In these calculations an energy minimum was found for Ge_{1.5}Sb₂Te₄. Experimentally, however, the resulting crystalline systems are described by the following formula, which relates the number of p-electrons per lattice site, *N_p*, to the stoichiometry (with *n_i* giving the number of species *i* per formula unit):

$$N_p = \frac{2n_{\text{Ge}} + 3n_{\text{Sb}} + 4n_{\text{Te}}}{n_{\text{Ge}} + n_{\text{Sb}} + n_{\text{Te}} + n_{\text{V}}} \quad (2)$$

Those compositions along the GeTe-Sb₂Te₃ pseudobinary line that form stable phases correspond to a number of $N_p = 3$, with $n_V = n_{Te} - (n_{Ge} + n_{Sb})$ (i.e., by balancing the mismatch between the number of anions and cations by intrinsic vacancies). At the same time, this vacancy concentration is required to establish the vacancy layers. The mismatch between the composition for which the energetic minimum is obtained in density functional theory-calculations, Ge_{1.5}Sb₂Te₄,^[27] and the experimentally obtained stable composition, Ge₁Sb₂Te₄, might be indicative of a connection between the aforementioned ordering of the sublattices (i.e., the setup of the cationic sublattice employed in the calculations) and the stable stoichiometry.

2.1.7. The Significance of Octahedral Arrangements

If one looks at a single structural motif that all crystalline phase-change materials have in common, one immediately notices the octahedral-like atomic arrangement. This finding of proximity to an—counting the number of valence electrons—over-coordinated structure (cf. “hypervalency”) and the occurrence of competing Peierls-like distortions, that turns out to be a structural fingerprint of phase-change materials, has important consequences for the electronic structure of phase-change materials as we will see in the following sections. Thus, the quantification of the distortion is an important aspect of structure investigation in the field of phase-change materials. Hence, it is not surprising that many studies have addressed the magnitude of these distortions. The simplest approach is to compare the lattice constant of the rocksalt-type structures with the actual bond lengths. These may for instance be obtained from EXAFS measurements^[28] or neutron diffraction data.^[29] A split of the six initially equal Ge-Te and Sb-Te bonds (recalling the principal octahedral coordination and atomic alternation) is observed, with distortions of approximately 0.2 Å per atom. Further quantifications have been given by means of computer simulations by various authors.^[30–33]

2.2. Electronic Structure of the Crystalline Phase

2.2.1. Photoelectron Spectroscopy Studies

Based on the review of the crystalline structure of phase-change materials, we may now turn to the study of the functional behavior that is linked to the electronic structure in the crystalline and amorphous phase. Photoelectron spectroscopy ought to be ideally suited to track down differences for the occupied states. **Figure 5** shows XPS-spectra for (GeTe)_{1-x}(Sb₂Te₃)_x.^[34] Three features are visible in the valence band density of states. The s-like states of tellurium (C), as well as antimony and germanium (B) lie significantly below the p-like states of all three species (A). The latter are located around the Fermi-level and hence are responsible for the bonding.

It is somewhat surprising that the measured spectra for the amorphous and crystalline state look quite similar. This raises the question, how the pronounced optical contrast between both states could be explained. It is not obvious, if the small differences in the valence density of states are sufficient to cause the optical contrast between the amorphous and crystalline state

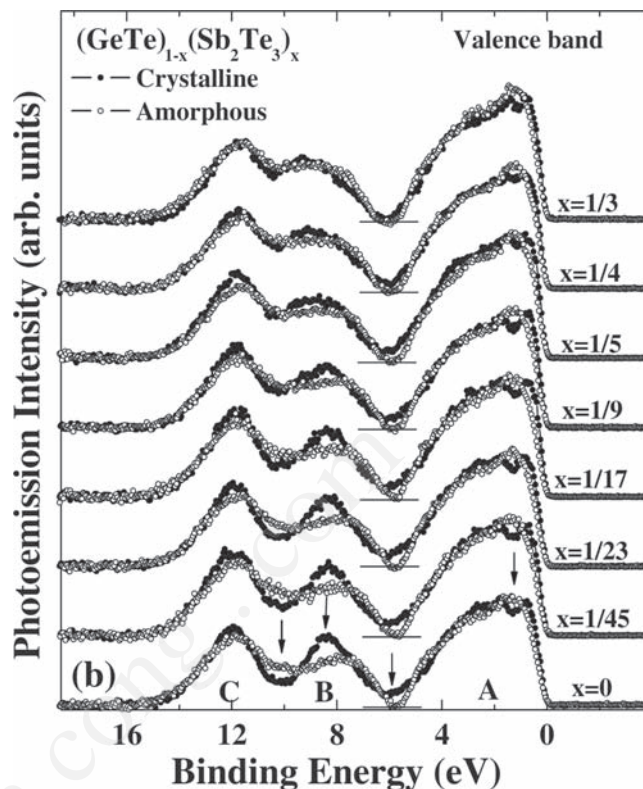


Figure 5. The valence band density of states of materials composed as (GeTe)_{1-x}(Sb₂Te₃)_x have been obtained by means of XPS for both the amorphous and crystalline phases. The s-like states (B,C) lie well below the occupied p-like states (A). Only minor differences between the amorphous and the crystalline state can be observed. Reproduced with permission from ref. [34]. Copyright 2007, the American Physical Society.

that every user of rewritable optical disks can notice. This task is not only of academic interest, but also has been the motivation of a significant amount of application driven material research. With every new generation of optical storage devices it had to be verified that the chosen phase-change materials had sufficient optical contrast at the new wavelength of choice [see Ref. 35 and references therein].

2.2.2. Optical Properties and the Origin of the Optical Contrast

Hence, the optical properties, that also probe the density of unoccupied states, have been investigated experimentally by many groups,^[24,36–38] but also theoretically.^[24,39,40] In the visible range between approximately 1.5 and 3.1 eV, the dielectric function is governed by the interband absorption over the electronic gap. From an extrapolation of the measured spectra it had been extrapolated that in comparison to the amorphous phase, the optical gap is typically smaller, with values of 0.2 to 0.6 eV for the crystalline phase. Hence, the gap falls below the typical lower boundary of the energy range that is accessible to ellipsometry.

Recently, Welnic et al.^[39] have found a microscopic explanation for the pronounced optical contrast employing time dependent DFT calculations. They could demonstrate that beside the decrease of the gap size, there is a pronounced

change of the matrix elements for the optical transition from the valence to the conduction band upon crystallization. It is usually assumed that upon crystallization there is mainly a change in the density of states, but changes in the optical matrix elements are frequently ignored. Phase-change materials, however, differ significantly from the usual scenario. While this is an important insight, the computational complexity of these DFT calculations renders them of limited use for the development and optimization of new phase-change materials. This immediately raises the questions how novel phase-change materials can be identified and how such materials can be optimized efficiently. Interestingly enough, the simplest scheme that we are aware of utilizes the optical properties of phase-change materials in the infrared. This is somewhat surprising, since in this frequency range, phase-change materials possess a broad transparency window. Nevertheless, the optical properties even below the absorption edge of crystalline and amorphous phase-change materials differ significantly. This is shown in **Figure 6**.

The visual inspection of this figure reveals three differences between the spectra of the amorphous and the crystalline state of phase-change materials. The energy range where oscillations, which are indicative for the transparency of the phase-change film, are observed is larger for the amorphous state. This implies that the amorphous phase has a larger optical gap than the crystalline phase, confirming earlier extrapolations from optical spectroscopy data. In addition, even in the energy range below the bandgap, the crystalline films show absorption. This can be seen from the fact that the interference maxima are considerably below unity. Most likely this is due to some collective excitation of charge carriers as will be discussed in more detail below. No such contribution is visible in the spectra

of the amorphous phase. The most interesting difference, however, is the different spacing of the reflectance minima. Since in this sample geometry we are performing a simple interference measurement, the spacing of the reflectance minima is governed by the optical thickness, i.e., the product of the film thickness and the corresponding refractive index. The observation that the reflectance minima are much more closely spaced in the crystalline sample cannot be explained by the characteristic 5% decrease in film thickness upon crystallization, which would even lead to a corresponding increase in the spacing of the minima. Instead, the refractive index of the crystalline state has to be significantly higher than the refractive index of the amorphous phase. This distinctive difference can explain the pronounced optical contrast that characterizes phase-change materials. These observations are reflected by the dielectric functions fitted to these spectra. Hence, these or similar measurements are ideally suited to identify and even optimize phase-change materials.

2.2.3. The Stoichiometry-Dependence of the Optical Contrast

How does this finding relate to the structure? In **Figure 7**, the atomic arrangement for a number of chalcogenides is displayed as a function of the average number of p-electrons per atom. This viewgraph shows that for an average number of 2 p-electrons per atom ($N_{sp} = 4$) a tetrahedral atomic arrangement is favorable, while for a larger number of p-electrons this atomic arrangement is destabilized with respect to an octahedral atomic arrangement. Filling an sp^3 -bonded system with more than 4 valence electrons requires the occupation of an antibonding orbital, thus the octahedral arrangement, where 5 valence electrons, and hence 3 p-electrons, can occupy bonding states is energetically favorable. All octahedral-like chalcogenides that have been measured so far^[41] show a high electronic polarizability in the crystalline state. This raises the question how the octahedral atomic arrangement that is promoted by the p-electrons leads to the high electronic polarizability.

2.2.4. Resonant Bonding

To understand the high electronic polarizability, this finding needs to be related to the electronic structure and atomic arrangements of these materials. We recall that there are about three p-electrons per site available to form covalent bonds in phase-change materials. Save for the atomic distortions, which will not be considered for the moment, the atoms are octahedrally coordinated. Thus, six covalent bonds are established, but there is an insufficient number of electrons to saturate these. This situation is very similar to the case of benzene. It is called resonant bonding (or resonance bonding)^[43] and is visualized in **Figure 8**. To elaborate the importance of this feature for phase-change materials, we shall discuss it in more detail.

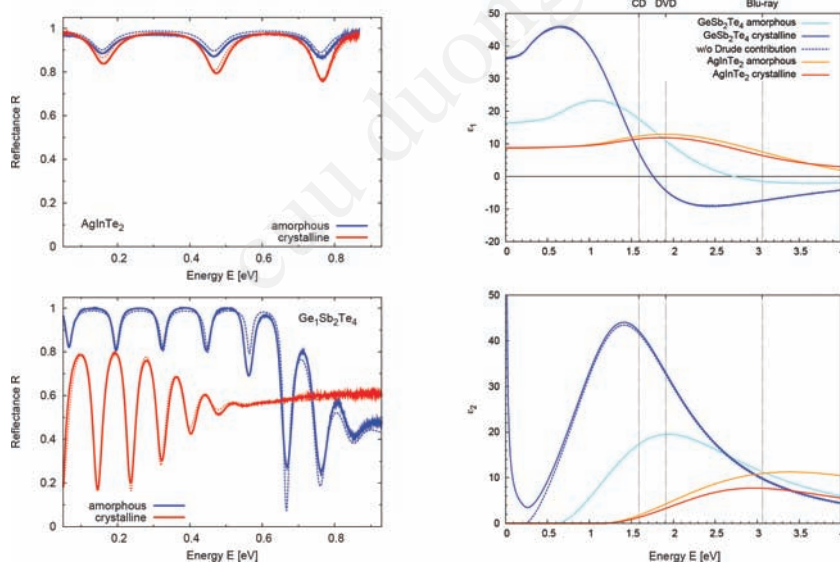


Figure 6. A combination of FTIR-measurements (left) and spectroscopic ellipsometry enables the simulation of the dielectric function of narrow-gap materials at and below the optical gap (right). The comparison between a non-phase-change material AgInTe₂, and a phase-change material, Ge₁Sb₂Te₄, highlights the unique properties of phase-change materials. Only the latter exhibit a significant contrast between the phases. In particular, the gap becomes smaller upon crystallization, and the optical dielectric constant, ϵ_{∞} , increases significantly. Data taken from ref. [41].

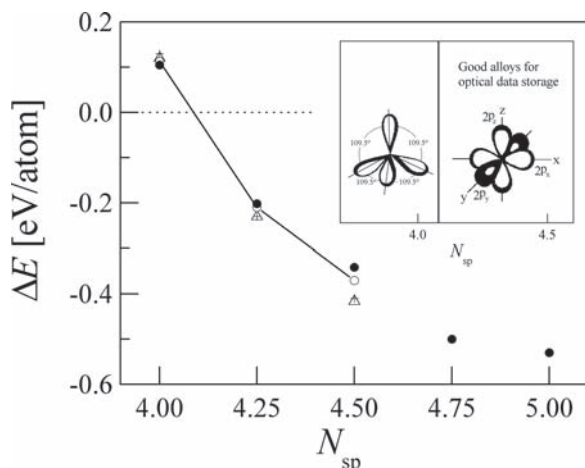


Figure 7. Te-containing materials with different average numbers of valence electrons have been studied by DFT-calculations. For each system, the energy difference between four-fold coordinated (chalcopyrite) and six-fold coordinated (rocksalt) structure were calculated. Materials with 4.25 and more electrons were found to form rocksalt structures. Reproduced with permission from ref. [42].

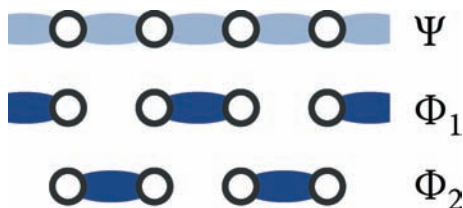


Figure 8. The essence of resonant bonding can be visualized using a simple linear chain of equal atoms. The strength of the shading of the covalent bonds symbolizes their saturation. The electronic wavefunction of the undistorted system, Ψ (top), may be expanded in a basis consisting only of saturated bond configurations Φ_i . The latter are energetically equal due to symmetry, that is “in resonance”. Thus, the situation drawn at the top corresponds to a superposition of these states. This electronic configuration is easily distorted by external perturbations. Reproduced from ref. [2].

Given that a suitable basis to expand the electronic wavefunction, Ψ , consists of saturated bond configurations, ϕ_i , then for a linear chain as shown in Figure 8, it may be expanded as

$$\Psi = \frac{1}{\sqrt{1 + \alpha^2}} (\phi_1 + \alpha\phi_2). \quad (3)$$

Since all basis configurations ϕ_i are energetically equivalent due to symmetry,

$$\langle \phi_1 | H | \phi_1 \rangle = \langle \phi_2 | H | \phi_2 \rangle = E_0, \quad (4)$$

that is in resonance, the term *resonant bonding* was coined. The total energy is lowered by the resonance energy E_{12} ,

$$E_{12} = \langle \phi_1 | H | \phi_2 \rangle. \quad (5)$$

Resonant bonding leads to a pronounced coupling of the electronic configuration to distortions via α .^[43] Thus, the

occurrence of resonant bonding is accompanied by a pronounced response of the system to atomic movements or electric fields, for instance. As a result, anomalously large Born effective charges, Z_T , and dielectric constants, ϵ_∞ , prevail^[18,43] (and references therein). The finding of large values of ϵ_∞ in phase-change materials serves as one proof of the occurrence of resonant bonding. Closely related are the rather small bandgaps –generally, ϵ_∞ increases with decreasing bandgap. However, a small gap alone is not sufficient, as in addition also the matrix elements of the optical transition (cf. Fermi’s Golden Rule) must be large to produce the significant electronic polarizability enhancement observed in phase-change materials. The works by Welnic et al.^[39] and recently by Huang and Robertson^[40] show that structures that support resonant bonding, in particular the crystalline phase of phase-change materials, lead to such high transition matrix elements. Other structures (orthorhombic GeS-type structure, spinel, ...) do not give rise to resonance effects since they lack resonant bonding or likewise the alignment of p-orbitals.

Resonance effects are a generic fingerprint of crystalline phase-change materials and the corner stone of the optical contrast employed in phase-change devices. These effects, however, are reduced by Peierls-like distortions. Hence, resonant bonding is endangered by these atomic displacements. From the point of view of orbital alignment, it is clear that distortions lead to misalignment. In terms of the expansion into saturated bond configurations presented above, a static atomic distortion favors one configuration over the other and thus counteracts the resonance. Nevertheless, for small distortions resonance effects are weakened but prevail; density functional perturbation theory calculations on GeTe prove, that, while the Peierls-like distortion and the subsequent cell distortion significantly reduce the values of Born effective charge and optical dielectric tensors, they nevertheless remain anomalously large.^[19] Therefore, it is proposed that the search for phase-change materials may be directed to those materials that exhibit resonant bonding and only a limited level of distortion.

2.2.5. Stoichiometry-Dependence of the Occurrence of Resonance

In order to assist this search rule, it is desirable to have a simple theoretical scheme that enables a prediction on whether a material may be expected to exhibit the desirable characteristics prior to characterization. Such a scheme has recently been proposed.^[19] Based on the work by Littlewood^[18] (and references therein), a two-dimensional map is constructed. It is spanned by two coordinates,

$$r'_\sigma = \underbrace{\left(\frac{\sum_i n_i r_{p,i}}{\sum_i n_i} \right)}_{\text{Anions}} - \underbrace{\left(\frac{\sum_j n_j r_{p,j}}{\sum_j n_j} \right)}_{\text{Cations}} \quad (6)$$

$$r_\pi^{-1} = \left[\underbrace{\left(\frac{\sum_i n_i (r_{p,i} - r_{s,i})}{\sum_i n_i} \right)}_{\text{Anions}} + \underbrace{\left(\frac{\sum_j n_j (r_{p,j} - r_{s,j})}{\sum_j n_j} \right)}_{\text{Cations}} \right]^{-1} \quad (7)$$

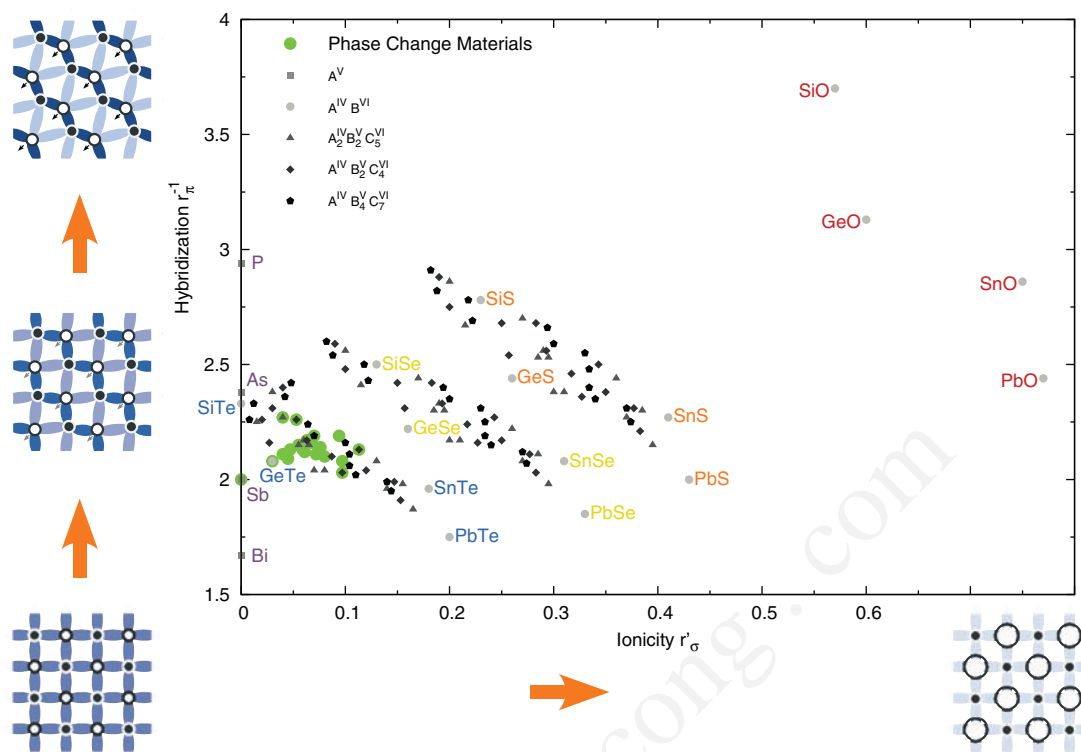


Figure 9. Empiric map for materials with about three p-electrons per atomic site and even numbers of anions and cations. The axes that span the map are the tendency towards hybridization, r_{π}^{-1} , and the ionicity, r_{σ}' , both defined in the text. The coordinates of a large number of materials have been calculated (see the supplement to ref. [19] for an index of materials). Phase-change materials are located within a small region of the map that is prone to the occurrence of resonant bonding. The graphs on the outside illustrate the weakening of resonance effects as one leaves this region due to the formation of less, more saturated covalent bonds via distortions or due to charge localization at the ions due to increasing ionicity. Reproduced with permission from ref. [19].

where the sums run over the anions and cations, respectively. n_i denotes the concentration of species i , while $r_{p,i}$ and $r_{s,i}$ refer to the radii of p- and s-orbitals, respectively. These radii are obtained from pseudopotential calculations. The first coordinate, r_{σ}' , provides a measure of ionicity. The second, r_{π}^{-1} , provides a measure of the tendency towards hybridization. For materials with approximately even numbers of anions and cations as well as $N_p = 3$, the resulting map is shown in **Figure 9**. The impact of both coordinates on the structures is shown by the schematic graphs at the border of this figure. An increasing hybridization favors distortions, which counteract the resonance character of the bonding. Increasing ionicity weakens the covalent (resonant) bonds at the expense of charge localization at the ion cores, and hence decreases the signature effects of resonance bonding. Thus, for resonant bonding with small distortions to occur, it is expected that only materials in the lower left corner have the potential to be employed as phase-change materials. Indeed, phase-change materials (marked in green) that have been identified empirically are found in this region. This underlines the potential of this simple scheme. However, it also shows that there is little room for finding better materials (with simple stoichiometries) than the ones already known. Future research may therefore attempt to transfer this scheme to other stoichiometries and other values of N_p . In that sense, the present two-dimensional map is only one projection plane

within a higher-dimensional composition space. Though, it is a particularly important one, since it hosts typical phase-change materials including antimony, GeTe and the Ge:Sb:Te-class as well as materials derived by isoelectronic exchange.

It has to be stressed that careful application of the map concept is advised. For instance, it is meaningless to put materials with an average number of p-electrons of two or four, or a pronounced deviation in composition from an equal amount of anions and cations such as e.g. SnSe_2 onto the same projection plane. Instead, a different projection plane should be chosen. Elements with d-states close to the Fermi-level are also not incorporated in the present scheme. Finally, the stability of a composition against phase separation also cannot be inferred from a map. Further information on the development of structure maps may for instance be obtained from the work of Pettifor.^[44]

To this point, we have identified the unique structure and bonding in the crystalline state as well as the resulting properties. From the studies of the electronic structure and the optical properties, we know already that the former is apparently similar in both phases, yet the latter is very different, enabling the use of phase-change materials in optical storage devices. Thus, along the lines of Sir Francis Crick, the question arises what structure the glassy phase exhibits in order to understand why resonance effects are limited to the crystalline phase.

2.3. Atomic Structure of the Melt

Since amorphization in phase-change devices proceeds via melt-quenching, it is clear that properties of the melt, such as its structure, are important for the understanding of phase-change recording. This is not only true since electrothermal modeling requires these properties as input, but also glass formation and structural properties of the glass must be expected to reflect properties of the liquid phase, since to a first approximation, a glass resembles a frozen-in liquid configuration. Therefore, it is evident that investigations of the liquid phase are important for the understanding of the amorphous phase and the kinetics of the phase transformation. To facilitate this, mainly molecular dynamics simulations as well as X-ray and neutron diffraction have been employed so far. Since the required elevated temperatures pose severe experimental challenges, the main focus is commonly on the structure.

The general result of these investigations, that are to be addressed in the following, is that materials successfully employed as phase-change materials are characterized by an octahedral bonding geometry of the atoms, with bond angles ranging around 90° . Related chalcogenides which do not show phase-change properties, on the contrary, deviate from this scheme, exhibiting tetrahedral sites with angles in the range of 109.5° as expected for sp^3 -hybridization. This finding has recently been obtained from neutron diffraction experiments performed on a wide range of phase-change materials and related materials by Steimer et al.^[45] These investigations revealed that only phase-change materials exhibited octahedral liquids. Moreover, the average number of valence electrons per atom was identified as an order parameter, with the octahedral-to-tetrahedral transition occurring at a threshold of about 4.25. Micoulaut et al.^[46] noted that an isoelectronic exchange can also impact the occurrence of tetrahedral coordination as they changed the stoichiometry from SnSe_2 to GeSe_2 , although this preserves the number of valence electrons.^[47] Furthermore, an

alternation between atomic species (e.g., ABAB) is observed in phase-change materials, resembling features of the crystalline structures as discussed later.^[32] So far it seems as if the octahedral-like atomic arrangement is the most important fingerprint of the structure of liquid phase-change materials. This is important since in recent years the identification of octahedral or tetrahedral bonding geometries in the amorphous and to a lesser extent the liquid phase has been a recurring motif in the literature.

It is interesting to note that the concept of Peierls-like distortions is also applicable to the melt. Experimental evidence for such distortions in liquid $\text{Ge}_{15}\text{Te}_{85}$ is given by neutron diffraction^[48] and X-ray absorption^[49] experiments as well as density functional theory simulations.^[50,51] Here, the liquid even becomes metallic if the opening of a gap in the density of states due to distortions is removed once the temperature is increased sufficiently high. Also in phase-change materials distortions are observed in molecular dynamics simulations, with their magnitude becoming more pronounced if the density is decreased.^[52] Molecular dynamics-simulations are progressively applied to a variety of liquid phase-change materials including AgInSbTe ^[53] and Sb_2Te_3 ,^[54] enabling a detailed study of their properties.

2.4. Atomic Structure of the Amorphous Phase

The structure of the solid amorphous phases of phase-change materials has been studied primarily by means of X-ray techniques that are sensitive to local atomic environments, e.g. extended X-ray absorption fine structure (EXAFS) measurements, neutron diffraction and molecular dynamics-simulations. With the amorphous phase of phase-change materials generally representing a covalently bonded network, the aim is to reveal the coordination number and the bonding geometry of each atomic species. This allows to assess the amorphous phase in terms of the previously introduced concepts and aids the understanding of the transition kinetics on an atomistic level.

Since most effort was put into research on prototype Ge:Sb:Te-materials, we shall focus on these results. From EXAFS measurements on GeTe and $\text{Ge}_2\text{Sb}_2\text{Te}_5$,^[55] it was found that chemical ordering takes place in the amorphous phase, leaving Te-atoms with germanium (and antimony) neighbors. The Ge-Te bond length was determined to be around 2.6 \AA and the coordination number of Ge was derived as four. Since the bonds could not be angular resolved, tetrahedrally coordinated germanium due to sp^3 -hybridization in GeTe_4 -configuration was assumed. The same result was later reported based on EXAFS- and XANES- (X-ray absorption near-edge spectroscopy) measurements.^[28] Further experimental support of this model was provided by X-ray fluorescence holography,^[56] Raman scattering studies,^[57,58] and density-functional theory calculations.^[59]

More detailed structural investigations have focused on resolving limitations of the X-ray-based studies. The combination with neutron diffraction data yields better contrast between Sb- and Te-atoms, that can hardly be distinguished by X-rays alone. The use of Reverse Monte Carlo method to simultaneously fit all data sets enables the simulation of the amorphous structure in large models, that allow for more than just a few local motifs and can statistically be evaluated. Employing this

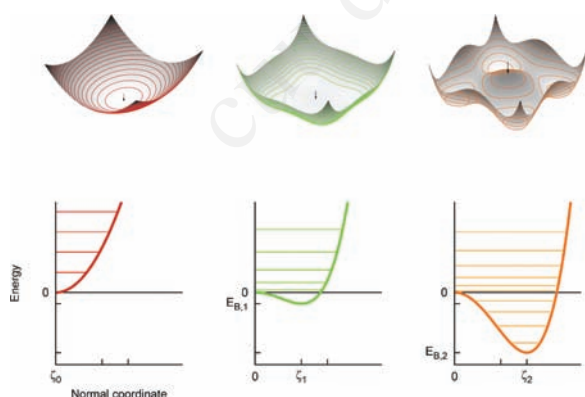


Figure 10. Peierls-like distortions lead to a peculiar shape of the energy landscape, that is the energy as a function of the atomic positions (in terms of a normal coordinate). From left to right, the undistorted case, a small, and a strong distortion are considered. The energy levels are indicated in the bottom row by horizontal lines. In the two border-cases the atoms only probe a rather harmonic potential at small temperatures. In the intermediate case, however, a pronounced anharmonicity affects the vibrational and thermal properties. Reproduced from ref. [2].

approach for as deposited-amorphous samples of $\text{Ge}_2\text{Sb}_2\text{Te}_5$ and GeSb_2Te_4 ,^[60,61] chemical ordering was confirmed. In particular, homopolar Te-Te- and Sb-Sb-bonds were ruled out, while a significant portion of Ge-Sb and Ge-Ge bonds was reported. Those were referred to as “wrong bonds” as they were not included in the original model. Coordination numbers were found to closely match the 8-*N*-rule. A predominance of the suggested GeTe_4 -tetrahedra was not obtained, leading the authors to reject approximations of the structure of the amorphous phase using simple local motifs. However, while the bond angle distribution for Te-Sb-Te showed a preferentially octahedral environment, the bond angle distribution for Te-Ge-Te indicated higher bond angles that are rather in line with tetrahedral environments.

The latter finding is in contrast to the expectation we infer from studies on the liquid phase, that indicate an octahedral structure also for germanium,^[52] but also to the results of another study of the amorphous phase. Kohara et al.^[62] performed Reverse Monte Carlo-simulations with synchrotron-radiation X-ray diffraction data for $\text{Ge}_2\text{Sb}_2\text{Te}_5$ and GeTe . For the former, bond angles around 90° and no homopolar bonds were obtained. Only for GeTe , both the presence of homopolar Ge-Ge-bonds and a deviation in bond angles from 90° coincided. Noteworthy is the analysis of the material topology in terms of *ring statistics*. A ring is defined “as the shortest closed path through nearest-neighbor atoms with each bond passed only once”.^[63] A predominance of even-numbered rings was found in $\text{Ge}_2\text{Sb}_2\text{Te}_5$. This finding is linked to chemical ordering, with an alternation of A (Ge/Sb) and B (Te) atoms in each ring. GeTe , however, exhibited an even distribution of even- and odd-numbered rings in line with the occurrence of homopolar Ge-Ge-bonds.

Due to the obvious differences between structure models derived from experiments alone, various large-scale molecular-dynamics simulations have been performed in recent years, enabling an unprecedented and detailed insight into structure and properties of the amorphous phase of phase-change materials. Materials investigated span the pseudobinary line $(\text{GeTe})_m(\text{Sb}_2\text{Te}_3)_n$ from GeTe ^[64,65] over $\text{Ge}_8\text{Sb}_2\text{Te}_{11}$ ^[66] and $\text{Ge}_2\text{Sb}_2\text{Te}_5$ ^[32,33,64,67-70] to Sb_2Te_3 .^[54]

The general result of these studies is a confirmation of chemical ordering, leading to the occurrence of 4-rings with pronounced AB-alternation. However, also a significant number of homopolar bonds as well as Ge-Sb bonds is obtained. Calculated bond-angle-distributions range primarily around 90° . Average coordination numbers suffer from both the ambiguity in selecting a cut-off distance as mentioned before, but also average over atoms in different environments. Yet, they tend to be larger than 8-*N* but smaller than six. Hence, the amorphous structure contains *defective octahedral* sites. In particular, germanium is found to coexist in both defective octahedral and tetrahedral environments, the latter comprising typically one third of the Ge-atoms in $\text{Ge}_2\text{Sb}_2\text{Te}_5$, that at the same time tend to be involved in homopolar (or Ge-Sb) bonds. Along the pseudobinary line, the concentration of tetrahedrally coordinated germanium increases towards GeTe , in line with the results inferred by Kohara et al.^[62] One further aspect is the presence of cavities in the amorphous network, that occupy an increasing amount of space as the antimony-concentration is increased. They may thus be regarded as precursors of the intrinsic vacancies of the crystalline phases discussed in

Section 2.1. We shall be concerned with the role of the ABAB-rings and cavities for the phase transition in Section 4.3.

By constraining the models according to experimental input, the level of agreement between simulation^[32,64] and experiments, namely X-ray photoelectron spectroscopy^[34] and high energy X-ray diffraction data,^[62] could be improved, though the qualitative result remained the same.^[69]

It is observed that coordination numbers—despite the ambiguity in defining them—tend to be larger than those derived from the 8-*N*-rule. However, a recent approach to define bonds based on a threshold for the localization of charges (measured by the electron localization function) rather than a threshold distance has been proposed by Xu et al.^[70] While the coordination of Te was found to be larger than two, Sb exhibited predominantly threefold-coordination. Germanium was obtained both in fourfold-coordinated environments, related to sp^3 -hybridization, and right-angled but only threefold-coordinated structures. Hence, while the coexistence of germanium in tetrahedral and octahedral sites is confirmed, the coordination numbers deviate both from previous reports and the 8-*N*-rule (if applied per species). Nevertheless, they all tend to be close to three, the number inferred from the 8-*N*-rule upon averaging all species. This method of defining bond numbers via electron localization promises to be more precise, though again ambiguity in defining a localization threshold remains. In order to link the results on coordination numbers to bond constraint theory, we may conclude that the variance in the published results prevents a unique comparison to the prediction of the 8-*N*-rule. Yet, a tendency towards higher numbers is found.

We shall not fail to remind of the fact that there is no unique amorphous phase, which affects the validity of comparisons between studies on amorphous solids. It may very well be that the extremely rapidly melt-quenched amorphous molecular dynamics-models differ in the concentration of tetrahedrally coordinated germanium, for instance, from as-deposited amorphous samples or melt-quenched samples used for experiments, or those amorphized by the application of hydrostatic pressure (see Section 4.3.3). Also, preparation conditions and structural relaxation (aging) are likely to affect structural, electronic and—in particular—electrical features. For instance, the electronic states around the gap can significantly depend on the quench rate.^[33]

We are now in a position to compare the atomic arrangement and the resulting electronic structure in the amorphous, liquid and crystalline state of phase-change materials. All phases are characterized by a predominance of octahedral coordination. This implies that bonding occurs mainly via p-electrons. Furthermore, there is an alternation between anionic and cationic species (“AB-alternation”). The structural similarities are reflected by the electronic structure. In this situation, where the phases between which switching is facilitated are so similar, the question arises what the pronounced contrast between them stems from. Yet, the answer was already given in Section 2.2.4, when we noted that the crystalline phase of materials that are successfully employed as phase-change materials are close to resonance conditions. This, however, is only feasible if distortions are small and medium-range order prevails. Hence, it is the crystalline phase that sets phase-change materials apart, at least as far as the property contrast is concerned.

3. Material Properties

In the preceding sections, a concept was developed which relates structure to bonding and the resulting optical properties. Now, our aim is to extend this framework to assess vibrational and thermal properties. Then, we review the current state of understanding of the electrical properties that these materials are characterized by, in particular the amorphous phase.

3.1. Vibrational and Thermal Properties

The lattice dynamics of the crystalline phase of phase-change materials have primarily been assessed by Raman-spectroscopy^[14,57,58] and density functional theory calculations.^[32,33,71,72] In addition, insight into the vibrational properties has been gained by analyzing Debye-Waller factors from structural investigations. Since Debye-Waller factors, B , serve as a measure of the “smearing” of atomic positions, they comprise two effects. On the one hand, the Peierls-distortion is typically subsumed as a static contribution. This approach is meaningful if isotropic atomic displacements from high symmetry-positions are assumed. On the other hand, a dynamical, temperature-dependent component reflects the thermal excitation of atomic vibrations. In the harmonic approximation, $B(T)$ factors are expected to exhibit a linear increase at elevated temperatures (temperature-derivative of the Bose-statistics). Debye-Waller factors have, for instance, been obtained by means of density functional-theory calculations by Caravati et al.^[33] (limited to the harmonic approximation) and X-ray diffraction measurements by Matsunaga and Yamada.^[73] In the latter work, even a super-linear increase at high temperatures has been obtained. Generally, the increase in the crystalline phase is larger than the one in the amorphous phase. This finding has been designated as a signature of phase-change materials, that is associated with the anharmonicity of the potential seen by the atoms due to the Peierls-like distortions, as visualized in Figure 10 [ref. 19 and references therein, ⁷⁴].

The vibronic properties of amorphous materials have been investigated for various reasons; experimentally, the observation of certain modes, for instance in Raman spectroscopy, may serve as fingerprint of the presence of corresponding local structural motifs such as GeTe_4 -tetrahedra.^[57,58] However, a possible shifting of the frequencies of such modes, for instance due to the environment of a local motif, leaves room for misinterpretation. Thus, the support by computer simulations proves useful. For instance, based on the analysis of the vibrational density of states projected onto different types of germanium atoms, tetrahedrally coordinated and homopolarly bonded germanium could be identified to be responsible for the energetically highest vibrational excitations in $\text{Ge}_2\text{Sb}_2\text{Te}_5$ ^[33] and in GeTe ^[75] Furthermore, merely as a side product of computationally expensive molecular dynamics simulations, also information on atomic diffusion constants (viscosity) is provided at certain temperatures given sufficient integration times.^[65,66] We shall revisit the structural dynamics in the amorphous solid in the discussion of the phase transition in Section 4.3.

The thermal properties of phase-change materials are of interest mainly for two reasons; as far as devices are concerned, knowledge about the heat propagation is of importance in

order to ensure low power consumption by heat confinement. It is also interesting to note that phase-change materials are very similar to thermoelectric materials. Bi_2Te_3 and PbTe , for example, are well established thermoelectrics, differing from Sb_2Te_3 and GeTe only by isoelectronic exchange. The figure of merit of thermoelectrics, Z , is defined as

$$Z = \frac{\sigma S^2}{\kappa}, \quad (8)$$

where σ is the electrical and κ the thermal conductivity, S is the Seebeck coefficient. A suitable material is characterized by a high electrical conductivity as well as small thermal conductivity. As for the electronic contribution, both are coupled by the Wiedemann-Franz law, so only the phonon-contribution to the thermal conductivity can independently be tuned. Besides strategies to pattern or stack materials in a way that additional phonon-scattering takes place (i.e., to enlarge the figure of merit by an extrinsic effect) it is also desirable to have a material that intrinsically exhibits small phonon lifetimes. Given our previous argument on the energy landscape of the crystalline phase, it is clear that anharmonicity due to Peierls-distortions may serve as such an intrinsic mechanism suitable to limit the lattice contribution to the thermal transport, a fact also noted by Rhyee et al.^[76] It is expected to be pronounced in materials further down in the map, so it is little surprise that PbTe for instance exhibits the desired properties. The map concept may thus be helpful to obtain materials suitable for thermoelectric applications.

Employing time-domain thermoreflectance measurements, Lyeo et al.^[77] have investigated the thermal conductivities of $\text{Ge}_2\text{Sb}_2\text{Te}_5$ in all phases. In the metastable crystalline phase, those are very low, adopting values on the order of $1 \text{ W m}^{-1} \text{ K}^{-1}$ (similar to window glass). Amorphous and metastable cubic phase differ by a factor of only about two. In both cases, the electronic contribution was found to be negligible. Differences were obtained between rapidly laser-crystallized and slowly oven-annealed samples. The former exhibited a smaller conductivity, ascribed to disorder. This is in line with the expectation of progressing ordering of the cationic site discussed before. Measurements of the thermal properties of phase-change materials have also been performed using the 3ω -method, yielding information on the behavior of the material itself but also at interfaces.^[78] Further measurements are reported by Giraud et al.^[79], Kuwahara et al.^[80,81] and Risk et al.^[82]

3.2. Electrical Properties

In recent years, the electrical properties of phase-change materials have attracted considerable interest as research shifted from optical to electrical memories. Consequently, the conductivity in both the crystalline and the amorphous state, in particular, shall be reviewed here. The fact that it differs significantly between the two phases, as the exemplary measurement of the resistivity in Figure 11 shows, allows to distinguish between logical states. In $\text{Ge}_2\text{Sb}_2\text{Te}_5$, for instance, the specific electrical conductivity at room temperature changes upon crystallization from $\sim 4 \times 10^{-3} \text{ } \Omega^{-1} \text{ cm}^{-1}$ to $\sim 1.5 \times 10^3 \text{ } \Omega^{-1} \text{ cm}^{-1}$, that is by six

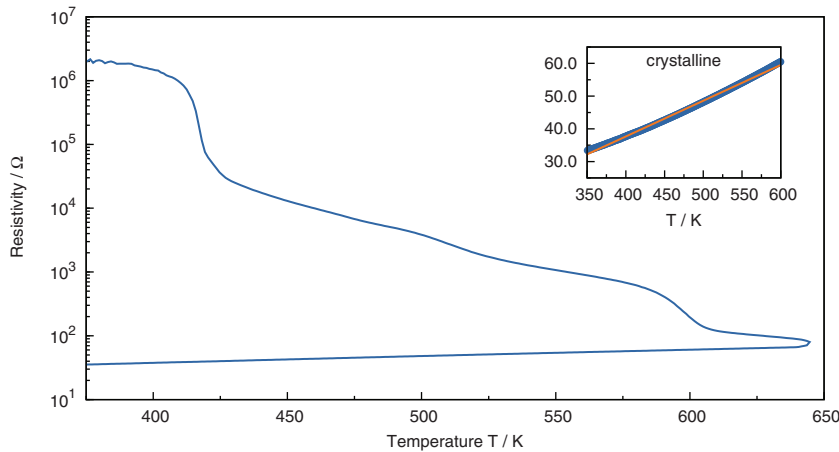


Figure 11. Shown are the phase transitions of a sample of $\text{Ge}_1\text{Sb}_2\text{Te}_4$ measured by the Van der Pauw-method. Crystallization occurs at around 420 K and leads to a significant drop in resistivity. A second irreversible, solid-solid transition is observed at about 600 K, which is identified as the transition from the metastable rocksalt- to the stable hexagonal phase. The charge transport in the amorphous phase is reasonably well described as thermally activated, while the crystalline phase obtained here exhibits a metal-like temperature-dependence (inset). (Data used with permission from M. Woda.)

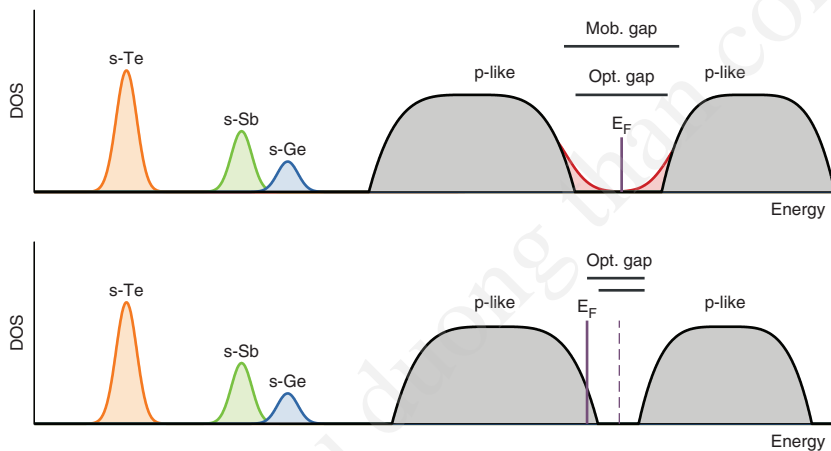


Figure 12. The schematic electronic densities of states of Ge:Sb:Te-materials in the amorphous (top) and crystalline (bottom) phase are compared. The s-states of the atoms are well separated below the p-like states. The latter are broadened and overlap. The optical gap of the amorphous phase is larger than in the crystalline state. Localized states (red) due to band tails (or defects) are found within the mobility gap. The Fermi level is pinned within the optical gap. In the crystalline state, the Fermi level is typically shifted towards or even into the valence band due to the formation of defects. Then, the optical gap exceeds the electronic gap due to the Burstein–Moss-effect. Reproduced from ref. [2].

orders of magnitude.^[83] Further analysis shows that the concentration of charge carriers in the crystalline phase is particularly high, reaching values on the order of $\sim 1 \times 10^{20} \text{ cm}^{-3}$.^[37] This is not a consequence of the small gap and thermal excitation, but induced by a pronounced shift of the Fermi-level towards or even into the valence bands due to defects. In anticipation of the results presented in this section, this indicates that the states around the Fermi-level and their nature dominate the electrical behavior of phase-change materials. **Figure 12** visualizes the principal situation in Ge:Sb:Te-materials.

3.2.1. Defects and Localization in the Crystalline Phase

For the crystalline phase, the most notable fact is that phase-change materials behave as extrinsic semiconductors. While plain narrow gap semiconductors are expected (and obtained in density functional theory calculations,^[39]), the Fermi-level is measured to reside close to or even within the valence band, giving rise to p-type conductivity.

This behavior is observed in a number of experiments. Measurements of the resistivity as a function of temperature show a change of slope from amorphous to the metastable and the stable crystalline phase. The change in the activation energy exceeds the change of the bandgap. When even a positive slope upon temperature increase is observed, the transition to a degenerate semiconductor becomes obvious.^[83] Due to this Fermi-level shift, free carriers are more easily thermally created in the crystalline state, yielding a Drude-like absorption in the infrared.^[84] In addition, the electronic gap might be (slightly) exceeded by the optical gap due to the Burstein–Moss-shift.^[37] Also in surface experiments, namely scanning tunneling spectroscopy, the shift of the Fermi-level is observed.^[85] Low-temperature Hall measurements have been conducted by Lee et al.^[37] The Hall-coefficient confirmed p-type conduction in the crystalline phase, and did not exhibit a freeze-out of carriers down to 5 K. Thus, for the investigated samples, the Fermi-level must have been within the valence band. Upon the metastable to stable crystalline phase transition, the charge carrier concentration increased by about 30%, but the mobility increase was much more pronounced. This has been attributed to a change in grain boundary scattering (cf. ref. 86). Furthermore, at high temperatures (above approximately 400 K) it was regarded insufficient to take into account only a p-component.^[37]

The Fermi-level shift towards/into the valence band in the crystalline phase has been attributed to the occurrence of defects. The case has been extensively studied for GeTe by Edwards et al.;^[87] the calculation of the

energy of formation of various defect types and charge states shows that particularly Ge-vacancies are easily formed, requiring little thermal energy. Depending on the position of the Fermi-level, these defects are (negatively) charged or neutral. With increasing temperature, the number of these defects increases. Concurrently, the Fermi-level is dragged towards the valence band. Though a definite, temperature-dependent concentration is expected in thermal equilibrium, the number might not vary with temperature on short timescales as predicted due to the temperature-dependence of the atomic mobility; if expelled

germanium aggregates at, e.g., grain boundaries, its diffusion back into the grain upon cooling appears unlikely. The presence of significant amounts of vacancies in the germanium-sublattice has been confirmed by EXAFS^[88] and X-ray diffraction.^[21] The same mechanism of defect formation, vacancies on the cation sublattice, is commonly anticipated to hold for other Ge:Sb:Te-based phase-change materials.^[33,87]

In a recent study a transition between thermally activated (non-metallic) and metallic transport has been observed in crystalline GeSb₂Te₄ with increasing annealing temperature. The non-metallic behavior has been attributed to a disorder induced localization in the metastable rocksalt-structure. At the transition to the metallic state, the corresponding electronic mean free path only amounts to 0.8 nm, which is interpreted as demonstrating a remarkably high level of atomic disorder.^[86] Furthermore, these authors suggest that controlling the degree of atomic ordering hence provides a mechanism to adjust the electronic properties.

3.2.2. Defects in the Amorphous Phase

Also in the amorphous phase, the position of the Fermi-level and the presence of defect states within the optical (or the mobility) gap have intensively been addressed throughout the course of phase-change material research. Consistently, the Fermi-level is found midgap for the amorphous phase, with evidence coming from the aforementioned photoemission spectroscopy (cf. Section 2.2) and molecular dynamics simulations (cf. Section 2.4), surface investigations via scanning tunneling microscopy^[85] as well as optical and electrical measurements addressed below. More specifically, the robustness of the position of the Fermi-level has been noted. Therefore, a microscopic picture explaining the pinning of the Fermi level is desirable, that can also be related to aspects of electrical conductivity. For chalcogenides, the model of valence alternation pairs (VAP) was proposed (see^[89] and references therein). Here, the deviation from two-fold-coordination of chalcogen-atoms "C", namely threefold-coordination that is unstable against the reaction $2C_3^0 \rightarrow C_3^+ + C_1^-$, creates a pair of acceptor-like and donor-like states, which thus pin the Fermi-level near midgap. Though attempts to apply this scheme to phase-change materials have been performed,^[90,91] the presence of VAPs in phase-change materials has been questioned by various authors. Robertson et al.^[92] noted that *mean* coordination numbers exceeding two, as shown for phase-change materials, rule out the occurrence of VAPs. MD-simulations by Caravati et al.^[33] could neither obtain tellurium-chains nor precursors of the required structures in Ge₂Sb₂Te₅. Furthermore, the absence of VAPs was concluded based on the absence of highly charged sites. As another result of this study, midgap-states were obtained only upon fast-quenching, localized at Sb-Te-chains.^[33]

Experimentally, electron spin resonance (ESR) measurements can illuminate the electronic state of defects. Singly-charged defects with non-zero spin exhibit microwave absorption upon the application of a magnetic field. However, unlike for conventional chalcogen-containing glasses such as As₂Se₃, no signal is obtained for amorphous GeTe and Ge₂Sb₂Te₅ (unless upon significant oxygen incorporation). That leaves the absence of defects or doubly charged defects as possible explanations. The latter

would be indicative of "negative U"-behavior, that is an overcompensation of Coulomb repulsion of the two carriers by the energy gain accompanying the distortion around the defect site.^[93]

To conclude, phase-change materials deviate from typical chalcogen glasses in their defect properties. No unique defect model for phase-change materials can be inferred from the literature. In contrast, the absence of characteristic states within the gap such as VAPs is advocated. In that case, one might only distinguish between two kinds of states in amorphous phase-change materials; states at the gap edges exhibit localization, whereas states within the valence (conduction) "bands" are extended. The two are separated by the so-called mobility edges. This finding is relevant for attempts to relate generic effects in the electrical conductivity to generic electronic (defect) properties.

3.2.3. Current-voltage-characteristics and Threshold Switching in the Amorphous Phase

One of the most active areas of research on phase-change materials is the electrical conduction. The motivation is sparked by the need to precisely control this material property in devices but also due to the scientific richness of the topic. Unlike optical properties, the electrical conductivity is very sensitive to all kinds of intrinsic and extrinsic parameters. It may therefore also serve as a probe of such parameters, though the results can be difficult to interpret given the variety of (possible) effects that have to be considered.

As a basic result of frequently conducted thin film resistance measurements, the electrical conductivity for small electric fields exhibits a thermally activated transport behavior,

$$\sigma(T) = \sigma_0 \exp(-E_A^{\text{cond}}/kT) \quad (9)$$

with an activation energy of approximately half the measured optical gap, $E_A^{\text{cond}} \approx 1/2 E_G^{\text{opt}}$. The exponential temperature-dependence, that might appear as a challenge for applications, does in fact not play a role. The contrast to the crystalline phase, discussed in Section 3.2.1, remains some orders of magnitude at all temperatures and is thus always sufficient to distinguish between the two states.

Another fingerprint of the charge carriers and the mechanism of their transport is provided by Hall- and Seebeck-measurements. From these measurements, the majority species of charge carrier transport can usually be deduced. However, respective measurements on Sb₂Te₃ and Ge₂Sb₂Te₅ by Baily and Emin^[94] and Baily et al.^[95] between 200 and 300 K yield opposite signs for both techniques. The Seebeck coefficient is large and indicates p-type conductivity. The Hall mobility is very low and anomalously signed (n-type). This is interpreted as an indication for conduction via hopping of small polarons (i.e., localized charges that trap themselves by distorting the surrounding atoms). Ielmini and Zhang^[96] argue that trap-limited transport is observed in phase-change materials. Such traps can be any kind of localized states close to the extended states, arising for instance as band tails. In this picture, charge transport takes place within extended states, but the mobility is significantly reduced since carriers are easily captured by unoccupied traps. The physical model for this mechanism is Poole-Frenkel conduction.

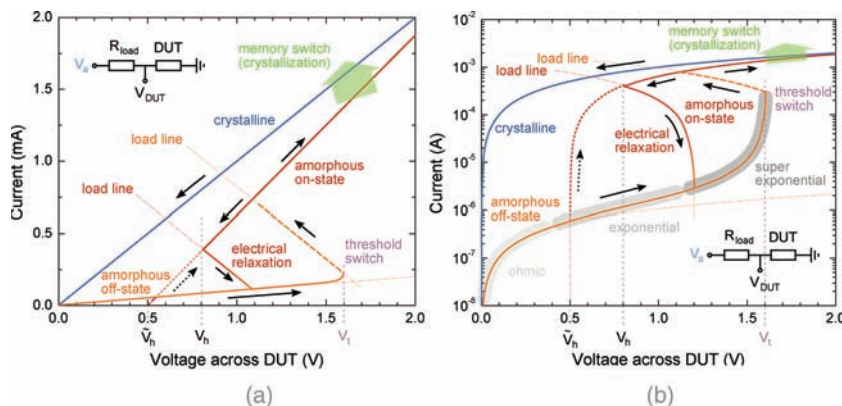


Figure 13. The current–voltage characteristics of phase-change materials (device under test, DUT), shown schematically in both linear (left) and logarithmic scaling (right), exhibit an interesting effect called threshold switching. For small electric fields the curves of the low resistive, crystalline and the high resistive, amorphous phase differ significantly. However, the situation changes if a critical voltage (corresponding to a field strength of some ten V/ μm) is exceeded. The amorphous phase suddenly becomes much more conductive, switching to the so-called ON-state as opposed to the OFF-state. This effect, called threshold switching, enables sufficient joule heating for crystallization (memory switching) at moderate voltages. Further aspects of threshold switching marked in the graphs are discussed in the text. Reproduced from ref. [99].

The litmus test of all models describing charge transport in amorphous phase-change materials, however, is whether they can account for the behavior at elevated fields. The electrical conductivity of amorphous phase-change materials exhibits a pronounced dependence on the strength of the applied electric field as shown in **Figure 13**. Two states can be discerned, the amorphous OFF- and ON-states. Until a critical field is reached, the threshold field E_t (or threshold voltage V_t), the system remains in the OFF-state. Here, the conductivity remains small, and follows first a linear, then an exponential and finally super-exponential behavior. When the field exceeds the threshold value, the conductivity largely increases. In this ON-state, the conductivity shows a linear field-dependence. From a technical point of view, this behavior is very desirable since crystallization of an amorphous bit is facilitated via Joule-heating. Without the *threshold switching*, large voltages would need to be applied in order to drive a sufficiently large current for heating and thus crystallization to occur. Furthermore, threshold switching can be exploited for selector devices in electrical memories, cf. Section 5.2. Threshold switching is to be distinguished from *memory switching* that refers to crystallization, while threshold switching is a phenomenon specific to the amorphous phase and does not involve a structural phase transition.

Experimentally only applied voltages rather than fields can be measured, so studies on the threshold fields employing electric testers have concentrated on the determination of voltages. If the geometry of the amorphous volume is known as in the as-deposited amorphous phase, the material-dependent field can be calculated from the voltage. It is typically about some tens of volts per micrometer (see ref. 89 and references therein, 97, 98). This enables threshold switching and thereby the operation of phase-change devices at voltages as small as about 1 V for phase-change cells with a distance between the electrical contacts of about 100 nm (neglecting voltage drops at the interface to the electrodes).

The discovery of threshold switching for data storage devices dates back to the pioneering work by Ovshinsky,^[1] and many

models have been proposed to account for it ever since. Sophisticated experiments have been designed to probe various aspects of threshold switching. Three of the key characteristics shall be summarized.

1. Threshold switching occurs upon reaching the critical field strength only after a delay time.

2. After the threshold switch, the ON-state is retained unless the field strength drops below a holding field strength E_h .

3. Shortly after the ON-to-OFF transition, an electric field E with $E_h < E < E_t$ is sufficient to recover the ON-state.

Most authors suppose that threshold switching is an electronic (rather than a thermal or structural) effect. Emin^[100] concludes that at elevated fields, the density of small polarons becomes larger. Thus, due to their proximity, lattice deformation becomes unfeasible once the threshold field is reached. Therefore, carriers may not localize anymore and the material becomes highly conductive.

In the picture of Ielmini and Zhang,^[101] Ielmini^[102] (and references therein), that is Poole-Frenkel conduction, the electric field increases the probability of a carrier that occupies one trap to get to another one nearby. At low fields, this requires extended states. At the threshold field, however, also direct tunneling becomes possible, leading to the conductivity increase. Another model presumes that threshold switching stems from a field- and carrier density-dependent generation mechanism, thus providing a positive feedback once a critical field is attained. At low fields, however, recombination counterbalances the generation.^[89,103,104] There are various possible microscopic models that could account for this phenomenological effect such as impact ionization.^[105]

An alternative to the electronic models of threshold switching is provided by field-induced nucleation.^[106] It is argued that at the threshold field, a crystalline filament forms in the amorphous volume, connecting the electrodes. The origin of this effect is ascribed to a field-dependence of the free energy of the system. Depending on the size of the filament, it is either stable or collapses upon removing the external potential.

A more detailed comparison between these models (and others not presented here) is beyond the scope of this review. The interested reader is referred to refs. 99,107,108.

3.2.4. Conductivity Drift in the Amorphous Phase

An issue important for multi-level storage is the drift of the amorphous resistivity with time. Multi-level storage aims at increasing the storage density by differentiating more than two logical states per cell. This is done by varying the volume of the amorphized part of the cell. However, one finds that the resistivity of a (partially) amorphous cell steadily increases with time. Multi-level storage is only feasible, if this drift is confined to a small resistivity interval associated with one logical state. The increase obeys a power law dependence on time. The process is thermally activated, and can thus be accelerated by raising the temperature.

Since progressing crystallization is expected to lead to a drop in resistivity as the crystalline phase has a lower resistivity, a different mechanism has to be identified. Moreover, since also threshold voltages tend to drift in the same fashion, a common origin of both effects is anticipated. There are several models that can account for the resistance drift effect. At any rate, it is desirable to identify an atomistic model for the structural rearrangement, that obviously occurs in this non-equilibrium phase, and to understand its impact on the material properties that surface in the observed drift. Yet, this topic is still up to debate. Most authors consider a general time and temperature-dependence of the parameters entering Equation 9, in particular of the activation energy [see ref. 109 and references therein].

On the one hand, a change in the size of the electronic gap due to stress relief has been discussed. In this universal model, the density difference between amorphous and crystalline state leads to hydrostatic pressure that is exerted on the amorphous volume after quenching. This causes the gap and thus the activation energy to decrease. The recovery of the gap then leads to the observed drift.^[90] This model has been further advocated by Karpov et al.^[110] In line with the model of stress relief, very small drift coefficients were obtained for Ge₂Sb₂Te₅-nanowires with exposed surfaces, that is non-confined structures as opposed to typical thin-films, in a recent study by Mitra et al.^[111]

On the other hand, models involving a change in the occurrence of particular electronic states have been proposed. More specifically, the presence of VAPs and an increase in their number, resulting in an increasing resistivity, have been suggested.^[90,91] This, however, is to be contrasted with the unsuccessful search for VAPs in phase-change materials discussed in Section 3.2.2. Another model (see ref. 112 and references therein) also aims at localized states at the gap edges, that might arise as tails rather than defects. Charge transport via hopping involving these states is hampered if the density of these states decreases. If the states vanish due to structural relaxation, a decrease in the hopping-conductivity results as the resistance drift. In addition, the position of the Fermi-level may be expected to move towards midgap given that it had previously been pulled towards one edge by these states.

4. The Phase Transition

After the discussion of the properties of both the amorphous and the crystalline phase in the preceding sections, we will now turn to the actual process of phase transitions, that is amorphization and crystallization. While the properties in both phases govern the contrast, the kinetics of the phase transition determine the stability of the states (data retention) and the transition times (device speed). A detailed understanding of the transition kinetics and the stoichiometry dependence is a necessity for the design of phase-change devices and suitable materials. Thus, a more detailed view on the phase-change cycle introduced at the beginning of this review shall be presented here.

Therefore, **Figure 14** shows the phase transitions in terms of a so-called time-temperature-transformation diagram. As this figure describes, the principle of phase-change recording relies on a peculiar interplay of the temperature-dependent atomic mobility (macroscopically observed as the reciprocal of the viscosity η) and Gibbs free energy G . The difference in G between the phases is the driving force for phase transitions; in equilibrium, the phase that minimizes G is adopted, but on small timescales, the finite atomic mobility kinetically hinders the establishment of equilibrium conditions. This enables the preparation of glassy bits by “freezing” a configuration of the undercooled liquid. Small atomic mobilities at ambient temperatures are also a key requirement for the stability of an amorphous bit. On the contrary, the mobilities must not be small at elevated temperatures to enable fast crystallization.

In the following sections, we will first focus on the process of amorphization via melt-quenching, and relate the kinetic properties of the undercooled melt and the amorphous state to their structure. Subsequently, the process of crystallization, which is typically limiting the maximum write rate of phase-change materials, is addressed.

4.1. Amorphization and Glass Physics

4.1.1. Glass Formation

As a melt is quenched, it becomes increasingly rigid. Once a critical temperature, the glass transition temperature T_g , is passed and given that crystallization has been avoided, the atomic mobilities D become too small for structural rearrangements required to reach thermal equilibrium. Thus, the undercooled liquid is “frozen in” in its current structural

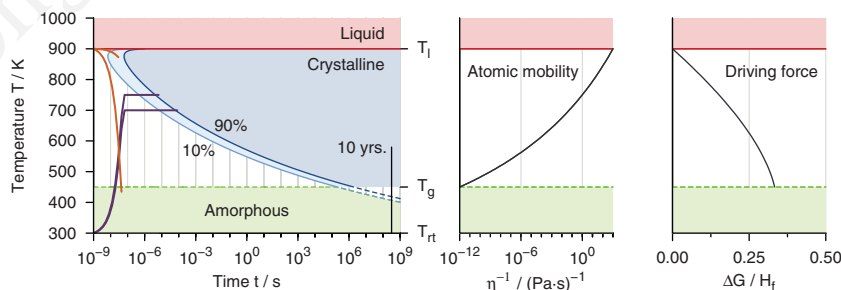


Figure 14. The graph on the left schematically shows the transformation of a fixed volume of a phase-change material depending on the time spent at a certain temperature. The crystallization of 10 (90) percent of the material is indicated by the thin (thick) blue lines/areas. As one cools the melt below the liquidus temperature T_l (typically around 900 K), the atomic mobility, related to the reciprocal viscosity shown in the middle, is very large. However, since the driving force for crystallization, that is the difference in Gibbs free energy between (undercooled) liquid and crystal, visualized on the right in units of the heat of fusion H_f , is small, crystallization does not take place immediately. It may thus be bypassed, if the melt is quenched sufficiently fast. This is visualized by two constant rate-quenching processes starting at T (orange), the slower of which leads to partial crystallization. Typically, quenching rates of 10^{10} K/s are required. At low temperatures, the driving force becomes larger, but the vanishing atomic mobility kinetically hinders crystallization. Eventually, as the glass transition temperature T_g (typically ranging around half T_l) is passed, an amorphous bit is formed. While ideally it is long-time stable against crystallization at ambient conditions, it crystallizes in fractions of seconds if the temperature is elevated and kept for a sufficiently long time. Two annealing processes starting at room temperature T_{rt} are indicated (purple). Obviously, crystallization time and temperature are mutually dependent. Reproduced from ref. [2].

configuration. The glass transition temperature is commonly defined as the temperature, at which the viscosity equals 1×10^{12} Pa s. The microscopic atomic mobilities of a liquid can be inversely related to the macroscopic viscosity η via the Stokes-Einstein relation,

$$D(T) \propto T/\eta(T). \quad (10)$$

The resulting glass is out of thermal equilibrium. Thus, a glass is always subject to “aging” effects, evidencing the relaxation towards equilibrium conditions. The timescale of these relaxations can be controlled by temperature. Nevertheless, depending on the stoichiometry of the corresponding glass, differences in the degree of aging are observed as will be briefly addressed later.

To assess the ease of glass formation, it is instructive to note that the shape of the area in Figure 14 that refers to crystallization is strongly affected by the temperature-dependence of the viscosity as we will address in detail in Section 4.2. Whether a glass can be formed at small cooling rates (*easy glass former*) or whether this may only be accomplished via rapid quenching (*marginal* or *bad glass former*) as in the case of phase-change materials, can thus be linked to the viscosity. Equivalently, it also relates to the speed of crystallization. The temperature-dependence of η varies among materials as is shown in Figure 15. If it is Arrhenius-like, a material is said to have a *strong* liquid. However, many materials exhibit a behavior empirically described by the Tamann–Vogel–Fulcher ansatz

$$\eta(T) = \eta_0 \cdot \exp(A/(T - T_0)), \quad (11)$$

with η_0 , A , and T_0 being constants. Such liquids are referred to as *fragile*. As a measure of the deviation from Arrhenius-behavior, the fragility m is introduced as a steepness-index at T_g via

$$m = \left. \frac{\partial(\log_{10} \eta)}{\partial(T_g/T)} \right|_{T=T_g} \quad (12)$$

A detailed review of these aspects has been given by Angell et al.^[13] Given that the viscosity at both T_g and T_l would be fixed, crystallization upon cooling of a strong (undercooled) melt is more likely bypassed even at moderate cooling rates as

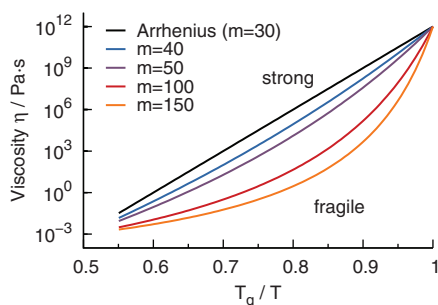


Figure 15. The viscosity of a liquid typically depends exponentially on temperature. If the dependence is Arrhenius-like, it is called a strong liquid. If the dependence at T_g is steeper, the liquid is referred to as fragile. The deviation from Arrhenius-behavior is indicated by the steepness at T_g , that is the fragility m . Reproduced from ref. [2].

compared to the case where the melt is a fragile liquid. Hence, a link between fragility and the ease of glass formation can be drawn. For phase-change applications, a rather fragile liquid appears favorable since the crystallization speed would increase more rapidly with increasing temperature (above T_g). However, the selection of a material with a fragile liquid over one with a strong liquid is, of course, only reasonable if both the normalized temperature-dependence and the absolute values of T_g as well as the atomic mobility at elevated temperatures are suitable for operation.

The term “glass” is originally reserved for amorphous solids that are formed by melt-quenching. As we will discuss later, materials may also be amorphous due to certain fabrication conditions or the application of pressure. Generally, the initial configuration might differ from that of a melt-quenched sample, possibly also resulting in different properties as the two are compared.

Glass transition temperatures can experimentally be assessed via differential scanning calorimetry since the transition from the glass to an undercooled liquid appears as an endothermic step. Such measurements have shown that for phase-change materials, T_g adopts values of about 450 K (i.e., approximately half the liquidus temperature).^[114] Empirically, this ratio between T_g and T_l characterizes phase-change materials as marginal glass formers [see ref. 115 and references therein]. The glass transition is easily obscured by crystallization, and is for practical reasons often estimated to be equal to the crystallization temperature T_c obtained upon heating with a moderate heating rate.

4.1.2. Glass Rigidity and Bond Constraint Theory

In order to design a phase-change material, it is desirable to have a theory that connects the stoichiometry with the structure but also with the glass forming ability. In Section 2.1 we have already addressed concepts to provide the link between stoichiometry and structure, discussing the 8-N-rule, as well as the role of distortions. In an attempt to relate glass forming ability with composition, we will briefly explain the concept of bond constraint theory. Such a conceptual framework for the description of the amorphous solid also holds the potential to clarify important aspects for phase-change materials such as the stability of the amorphous phase against crystallization, as well as aging due to structural relaxations.

Bond constraint theory is an approach to characterize the rigidity of an amorphous covalent network based on the (mean) atomic coordination. In order to fix an object at a given place, three constraints are required. If more constraints are present, the loss of one constraint does not generally lead to the release of this fixation. Less constraints, on the other hand, leave open degrees of freedom, giving room to limited movement (i.e., so-called floppy modes). It is hence reasonable to classify covalent networks such as glasses according to the number of constraints per atom, n_c . An *ideal* glass has a value of three, whereas *floppy* glasses have less and *stressed rigid* glasses have more constraints per atom. Moreover, bond constraint theory also provides a link between n_c and the experimentally accessible coordination number, r . Given that in a covalent network the number of bond-stretching constraints equals half the number of bonds and the respective number of bond-bending constraints sums up to $2r - 3$, then the relationship as proposed by Phillips^[116] reads

$$n_c(r) = \frac{5}{2}r - 3 \Leftrightarrow r = \frac{2}{5}(n_c + 3). \quad (13)$$

This implies that in an ideal glass, $n_c = 3$, the average coordination should take the value 2.4. Vice versa, since the average coordination is often characteristic for an atomic species, cf. the 8- N -rule, changing the stoichiometry of a glass allows to modify r and thereby to affect the rigidity of the glass. Recently, it has been argued that floppy and rigid glasses are not separated by a unique point, but rather a continuous regime, the so-called intermediate phase. Thus, instead of one there are two rigidity transitions upon variation of r as evidenced by experiments for chalcogenide glasses, with the intermediate phase marking a range of *isostatic* rigidity.^[117] Interestingly, a link between rigidity of the glass and the temperature-dependence of the viscosity of the liquid has been discussed. In Micoulaut et al.,^[118] it has been claimed that both floppy and stressed rigid glasses exhibit fragile liquids, whereas intermediate glasses should exhibit strong liquids.

The conceptual complexity of the connections between rigidity, fragility, glass transition and the bond characteristics of a specific material sounds a note of caution when it comes to simplifications. Nevertheless, we want to provide an intuitive approach to the link between ease of glass formation and glass rigidity. The degrees of freedom present in a floppy glass (and the ease of thermal excitation of “floppy modes”) are favorable for crystallization, so that the glass forming ability fades as r tends to smaller numbers, and T_g decreases. As r increases—coming from the intermediate/ideal glass- T_g should to a first approximation become larger, since more thermal energy is required for structural rearrangements as more bonds are formed. However, the increase of the number of bonds can be overcompensated by a weakening of the bond strengths, giving rise to a non-monotonous behavior of $T_g(r)$. In addition, the increasing number of bonds becomes hard to form without what is called *bond mismatch*; the bond lengths deviate from the energetic optimum, which increases the energy of the glassy state and thereby also the driving force for crystallization. Consequently, the glass forming ability fades towards the stressed rigid regime.^[118]

Easy glass formation is thus expected only for ideal/intermediate glasses. This is unfavorable for fast crystallizing phase-change materials as argued before. Indeed, typical phase-change materials yield, according to the 8- N -rule, numbers of r between 2.6 and 3.2, locating them in the region of stressed rigid glasses. The coordination numbers derived from structural investigations (see Section 2.4) tend to be higher, so phase-change materials are seemingly even more stressed rigid than expected by the 8- N -rule. According the aforementioned link between rigidity and fragility,^[118] this should lead to a higher fragility of the liquid. Thus, bond constraint theory and its application to phase-change materials is currently investigated as a simple means of a priori material selection. However, the determination of r from the 8- N -rule can be insufficient as we have noted before. Hence, it may be determined experimentally or by simulation. In both cases, determination of r via integration of a pair distribution function (i.e., counting of bonds based only on atomic distances)

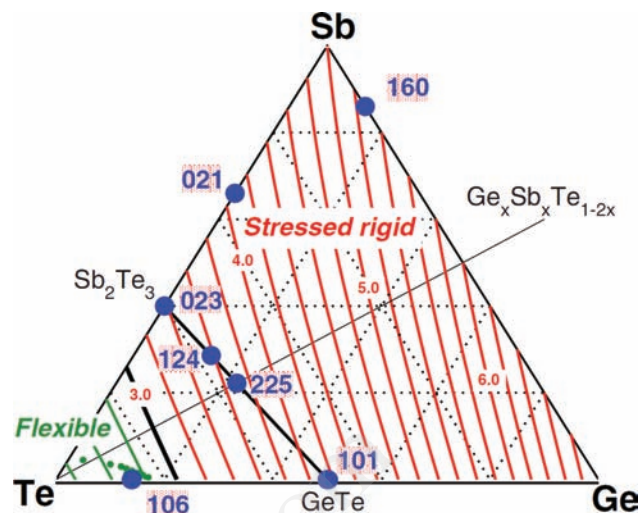


Figure 16. The contour lines within the ternary Ge:Sb:Te-phase diagram indicate the number of constraints n_c , and split the area into a floppy/flexible ($n_c < 3$) and a stressed rigid ($n_c > 3$) regime. Clearly, phase-change materials fall into the latter, highlighting that phase-change materials are bad glass formers. Reproduced with permission from ref. [121]. Copyright 2010, American Physical Society.

requires the selection of a cut-off-radius, which can lead to ambiguous results. A successful example of experimental confirmation of the predictions of bond constraint theory is given by Jovari et al.^[119] Here, $Ge_{15}Te_{85}$ was shown by Reverse Monte Carlo analysis of both neutron and X-ray diffraction data to have an average coordination number slightly above 2.4, in line with the expectation according to the 8- N -rule and its easy glass formation ability. Improving the counting of constraints to determine $n_c(r)$ based on r 's derived from EXAFS-data was proposed, but led to the controversial result that $Ge_2Sb_2Te_5$ was also an easy glass former,^[120] in contradiction to its fast crystallization behavior. More recently, extensive work on the rigidity and application of bond constraint theory in the ternary Ge:Sb:Te phase diagram has been presented by Micoulaut et al.^[121] Employing density functional theory calculations, these authors were able to prove that phase-change materials indeed fall into the stressed rigid regime as shown in **Figure 16**.

Due to the importance of T_g for data retention, a large body of work on phase-change materials is concerned with means of material modifications to increase the value of T_g . In general, a host phase-change material such as $Ge_2Sb_2Te_5$ or antimony is chosen for its optical and electrical properties in the amorphous and crystalline phase. Then, the impact of the addition of other elements is investigated. Theoretically, means of (semi-empiric) prediction of T_g have been proposed. For tellurium-based materials for instance, the application of the (modified) Gibbs-DiMarzio equation has been demonstrated to yield a trend for fixed concentrations of Te-content.^[122] This approach was originally proposed for chain-like structures such as polymers. It may hence be expected to work only for chalcogenide-rich materials, that retain the chain-like structure of elemental tellurium and selenium, but is not generally applicable to phase-change materials. A more universal model was proposed by Lankhorst^[123]

(see also ref. 124), that empirically relates T_g to the enthalpy of atomization of an amorphous network. The latter is calculated from the bond enthalpies of all bonds. It has been successfully applied to resolve the impact of Al- and Cu-doping on Ge:Sb and Sb:Te as evidenced by experiment.^[125] A complementary experiment on Al-doping of Ge:Te was conducted by Katsuyama and Matsumara.^[126] Here, it was also shown that a material composed only of Ge:Sb:Te forms a glass only in a relatively small compositional region close to $\text{Ge}_{15}\text{Te}_{85}$ upon liquid N_2 -quenching.

In the framework of bond constraint theory, the observed increase of T_g via the addition of so-called network forming elements, for instance from group IV, to a host phase-change material can be understood by the resulting increase of r . One important aspect not included in bond constraint theory, however, is the fact that not only the number of bonds, but also the bond energies need to be taken into consideration. Thus, the dependence of T_g on r via stoichiometry variation may deviate from a monotonous increase. That explains the success of the Lankhorst-model since it incorporates both bond numbers and bond energies. This, however, is facilitated at the expense of simplicity as for the bond energies the atoms participating in each bond need to be explicitly known. Hence, structural information on phase-change materials in the solid amorphous phase is required.

4.2. The Process of Crystallization

Two mechanisms of crystallization are discernible, nucleation and growth. Nucleation is the process of forming a crystalline nucleus within an amorphous matrix. By growth, the progression of the phase front separating amorphous and crystalline regions is referred to. This is visualized in Figure 17. The driving force for crystallization is the gain in free energy below the melting temperature. However, if a crystalline nucleus is formed in an undercooled liquid (amorphous) material, also an interface between the two states has to be created. The process of nucleation is typically modeled in a continuum-approximation, neglecting the discrete atomic structure. Then, the formation of a crystalline nucleus involves the formation of a continuous interface. We shall briefly review the modeling of nucleus formation and growth. Detailed information may for instance be obtained from refs. 127, 128.

It is found that the difference in free energy $\Delta G(r)$ for a spherical crystalline cluster of radius r within an undercooled melt is



Figure 17. From left to right, the crystallization (bright gray) of an amorphous film (dark gray) is shown. Due to the illumination with a laser beam, for instance, and the resulting increase in temperature, crystalline nuclei form in the amorphous matrix. The volume of these crystals steadily increases due to growth. Finally, both due to nucleation and growth, the amorphous bit is completely crystallized. Yet, it is typically polycrystalline, as the crystalline nuclei exhibit different orientations.

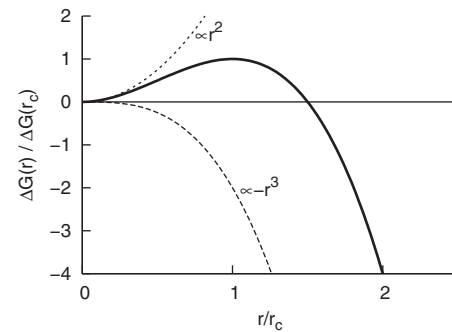


Figure 18. The formation of a crystalline nucleus (here, we assume a spherical shape) within an amorphous matrix is dominated by the interplay of the energy gain due to the volume ($\propto r^3$) of the nucleus and the energetic cost of establishing an interface ($\propto r^2$) between the phases. Only those nuclei that exceed the critical radius r_c due to thermal fluctuations tend to grow, whereas smaller nuclei tend to dissolve again.

$$\begin{aligned} \Delta G(r) &= V(r) \cdot \Delta G_V + A(r) \cdot \sigma \\ &= \frac{4}{3}\pi r^3 \cdot \Delta G_V + 4\pi r^2 \cdot \sigma \end{aligned} \quad (14)$$

with V and A being the volume and the surface of the nucleus, ΔG_V the difference in G between the two phases per unit volume and σ the interfacial energy per unit surface area. At the critical radius,

$$r_c = \frac{2\sigma}{|\Delta G_V|} \quad (15)$$

$\Delta G(r)$ exhibits a maximum. So only nuclei of a size greater than r_c gain energy by growth, see Figure 18.

Below this critical size, their dissolution is energetically preferred as it removes the interface (and hence reduces the free energy of the system). According to Becker and Döring, a steady-state distribution of subcritical clusters is formed after an incubation time τ . Recently, Lee et al.^[129] proposed fluctuation transmission electron microscopy to experimentally study the evolution of such subcritical nuclei in thin films (here AIST) upon laser irradiation. From the steady-state distribution, a steady-state nucleation rate I_{ss} given by

$$\begin{aligned} I_{ss} &\propto \eta(T)^{-1} \exp\left(-\frac{\Delta G(r_c)}{k_B T}\right) \\ &= \eta(T)^{-1} \exp\left(-\frac{16\pi}{3k_B T} \frac{\sigma^3}{(\Delta G_V)^2} \cdot f(\theta)\right) \end{aligned} \quad (16)$$

is derived. For the moment, we shall neglect the factor $f(\theta)$, thus setting it to unity. Once postcritical crystalline nuclei have been formed, their speed of growth for sizes $r \gg r_c$ is derived in the framework of classical crystallization theory as

$$u(T) = \frac{\partial r}{\partial t} \propto \frac{T}{\eta(T)} \left[1 - \exp\left(-\frac{\Delta G(T)}{k_B T}\right)\right]. \quad (17)$$

The temperatures at which nucleation and growth exhibit their respective peak values are not the same, and also one process might generally be more dominant than the other. Hence, nucleation-dominated and growth-dominated crystallization have been observed in the rather large volumes encountered in optical recording, leading to a sub-classification of phase-change materials. To a first approximation, the time it takes to crystallize an amorphous bit does not depend on its volume in the case of nucleation-dominated crystallization. Growth-dominated materials, on the other hand, do exhibit a volume dependence; the smaller the volume, the quicker it is completely crystallized.^[130] In general, the subclassification becomes less helpful for small volumes, where geometry and interfaces play a more important role, increasing the contribution of crystal growth to the transformation.

From this, it is clear that an appropriate description of crystallization kinetics of a phase-change material needs to consider and distinguish these two processes, that—though one might dominate the other—are always simultaneously present. The widely employed Kissinger-analysis does not separate the two and should for this reason be critically reviewed.^[128]

One can distinguish between three temperature regimes relevant for research on the crystallization kinetics. The first regime is located at around the glass transition temperature. In this temperature interval, crystallization is ought to proceed very slowly. For data retention, a ten years at 80 °C-requirement on the stability of a logical state is typically envisaged. Experimentally, the slow crystallization enables the direct observation of nucleation and growth.^[131] This has also been demonstrated using high-resolution transmission electron microscopy during annealing of Ge:Sb:Te-films.^[132,133] An alternative approach is the use of atomic force microscopy on isothermally annealed samples.^[134] This way, growth velocities of Ge₂Sb₂Te₅, Ge₄SbTe₅ and AIST have been obtained. They obey an exponential temperature dependence. From this knowledge, data retention at a given temperature can be assessed.

A second temperature regime of interest is situated just below the liquidus temperature. The small driving force for crystallization enables to study the undercooling of droplets employing differential thermal analysis. Here, the maximum undercooling is determined, that is the difference between liquidus temperature and the temperature at which crystallization occurs upon the application of a constant cooling rate. Combined with measurements of the heat of fusion, limits for the interfacial energy σ and the steady-state nucleation rate I_{ss} are derived. From their results, Kalb et al.^[135] concluded that steady-state nucleation rates were larger for Ge₂Sb₂Te₅ and Ge₄SbTe₅ than for Ge₁₂Sb₈₈ and AIST. This explains why the latter materials belong to the class of growth-dominated materials, whereas the former are nucleation-dominated. The main difference between the two groups was identified in the heat of fusion normalized to the liquidus temperature; the nucleation-dominated materials exhibit smaller values.

The experimentally most challenging yet technologically relevant temperature regime is located somewhere between liquidus and glass transition temperature, where crystallization proceeds the fastest. Insight into material characteristics may be gained here by two approaches. On the one hand, materials may just be tested under operation conditions. Either embedded

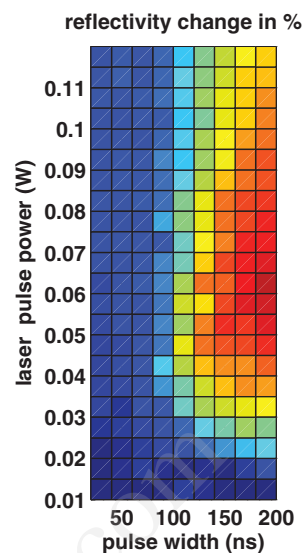


Figure 19. Power-time-effect diagram for optical characterization of the crystallization behavior of an as-deposited amorphous Ge₂Sb₂Te₅-film deposited on silicon. A laser pulse power of about 50 mW applied for only 150 ns leads to crystallization of the illuminated spot as evidenced by the pronounced change in reflectivity. Reproduced from ref. [128].

in production-type samples or using specialized equipment to spatially and/or temporally resolve the phase transition, the performance of a material and the suitability of the device geometry may directly be investigated. In particular, the minimum crystallization time is assessed this way. **Figure 19** shows an example of such an optical tester measurement in terms of a power-time-effect diagram. By the variation of the pulse in terms of power and time, different degrees of change in optical reflectivity (effect) are obtained. We will be concerned with such experiments for electronic memories in the final section.

On the other hand, information on the physical processes that lead to crystallization can be reconstructed also from the morphology of a crystallized bit.^[131,137,138] In particular transmission electron microscopy as presented by Kooi and De Hosson^[132] or Friedrich et al.^[136] – shown in **Figure 20** – yield detailed insight into the distribution and shape of crystallites, from which the distribution of nuclei and their growth can be inferred.

So far, we have only considered homogeneous phases. However, the activation energies can be affected by introducing heterogeneities. This is incorporated into the framework of crystallization theory by a factor $f(\theta)$, with θ being the wetting angle. Impurities and interfaces can catalyze nucleation, but also, they can hinder growth. If heterogeneous sites play a dominant role, crystallization shifts from being triggered in the whole volume of the material to the vicinity of these heterogeneous sites. Interfaces are almost inevitable in phase-change recording. In nanoscaled electrical devices, their presence in the vicinity of the active material cannot be avoided. But also homogeneous films of phase-change materials as employed for optical recording are strongly affected by interfaces despite their spatial extension. In fact, the choice of the dielectric capping material in optical discs^[139,140] or electrode material in electrical memory cells^[141] have been shown to significantly influence the crystallization behavior. The latter work highlights the

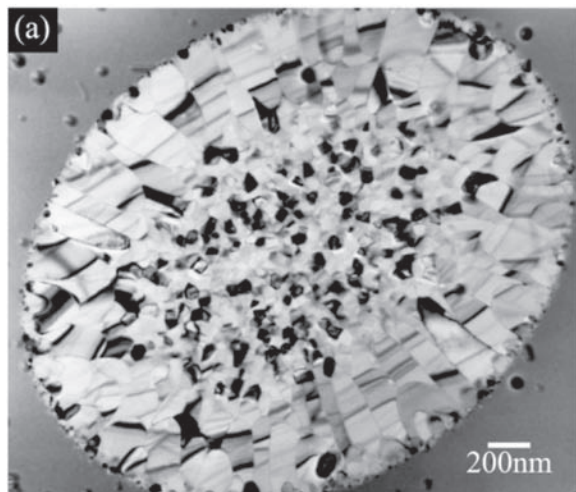


Figure 20. TEM image of a laser-crystallized spot in an otherwise as deposited-amorphous $\text{Ge}_2\text{Sb}_2\text{Te}_5$ -film. Reproduced from ref. [136]. Copyright 2005, Elsevier.

importance of such considerations in particular for thin films; below about 5 nm, crystallization temperatures are dominated by the choice of the interface material.

But not only the materials adjacent to the phase-change material play a role; by amorphization of a bit, a crystalline rim is created since the temperature gradient and thus the cooling rate becomes too small for amorphization at a certain distance from the center of the laser spot, the conductive filament or the heater element, respectively. Hence, the process of growth is typically decisive in electronic phase-change memories, also because no incubation time as for nucleation is involved.

Finally, the actual configuration of the amorphous phase itself has a pronounced impact on the crystallization properties. Particular structural features of an as-deposited amorphous phase, that are not present in a melt-quenched amorphous phase, might vanish for good after the first crystallization, and hence be irrelevant for applications that involve countless numbers of cycles. Various authors have noted that the first crystallization of an as deposited amorphous phase may be very different from re-crystallization of a melt-quenched phase.^[131,142–144] Thus, it becomes clear that one has to be very cautious about the exact experimental conditions and the comparability of experiments that state, for instance, crystallization temperatures.

As we have noted already in Section 4.1.2, tuning the crystallization kinetics by “doping” (stoichiometric variation) is routinely investigated in the field of phase-change materials. We refer the interested reader to the article of Zhou,^[145] who reviews the effect of addition of nitrogen or oxygen, for instance, on the crystallization behavior. Notably, two scenarios may be discerned; a nucleation-dominated material may crystallize faster if doped with a certain element. However, the same dopant may impede growth in a growth-dominated material.

4.3. Atomistic Modeling of the Phase Transition

In the previous section, we have employed the continuum approximation, neglecting the discrete atomic structure. The

energy barrier separating the phases has not been linked to stoichiometry and microscopic structure. Thus, it is desirable to improve the understanding of the crystallization kinetics by developing and testing atomistic models of the phase transition.

4.3.1. The Umbrella-Flip Model

A noteworthy model for Ge:Sb:Te-systems was given by Kolobov et al.,^[28] the so-called umbrella-flip model. It stated that the main structural rearrangement taking place upon crystallization is a flip of germanium from tetrahedral to octahedral sites. Since this model not only gave an intuitive explanation of why the phase transition proceeds so fast yet involved a change in bonding significant enough to account for the contrast observed, it attracted much attention. A lot of successive studies attempted to test this model.

The extensive theoretical simulations and experimental studies in recent years, that we have addressed in Section 2.4, have shown that, while tetrahedrally coordinated germanium-atoms are indeed present in the amorphous phase, they represent only a minority, making up only roughly one third of all germanium atoms. Also, they typically involve homopolar Ge-Ge or Ge-Sb bonds (“wrong bonds”) rather than only Ge-Te bonds as stated by the umbrella-flip model. Preparation conditions may have significant influence on the concentration of tetrahedral germanium. As for phase-change devices the performance after thousands of switches is of importance, the results obtained from melt-quenched samples appear to be most relevant. Another issue is that this model implicitly requires a certain atomic order or distortion pattern. Otherwise, the coordination of germanium would exceed four upon flipping from the octahedral site.^[146]

To conclude, the umbrella-flip model turned out not to be a realistic model of the phase transition. Though tetrahedral germanium is indeed present in the amorphous phase, it is not a universal motif. Moreover, this model does not apply to phase-change materials that do not contain germanium.

4.3.2. Evolution of Ring Statistics During the Phase Transition

Though a simple local structural scheme like the umbrella-flip model is appealing, it is unlikely that such a model realistically or universally accounts for the phase transition in phase-change materials. Thus, we might turn to another qualitative, more statistical evaluation of the structural differences. Based on the current state of structure assessments (cf. Section 2.4 and Section 2.1), it is noted that both phases share structural features such as AB-alternation and preferentially octahedral coordination. To a first approximation, the amorphous phase represents a strongly distorted copy of the crystalline phase. The strong distortion, that significantly exceeds the level present in the crystalline phase, destroys the mid-range order and removes the resonance character of the covalent bonds (or misaligns the orbitals^[40]). Thus, the characteristics of resonant bonding, such as large values of ϵ_∞ , do not prevail in the amorphous phase. This model may universally be applied to phase-change materials as it does not rely on the presence of certain species such as germanium.

Similar to the line of reasoning in the umbrella-flip model, one might suspect that the rapidness of crystallization stems from the fact that only a small change in structure is required, that is the reduction of the strong distortions. In fact, the presence of the metastable crystalline phase, that only successively orders to eventually transform into the stable phase, shows how little “medium-ranged” diffusion takes place upon crystallization. The erasure of “wrong bonds” and the tetrahedral portion of Ge-atoms appears to be the most significant rearrangement and likely impedes fast crystallization. Nevertheless, apparent structural similarities or differences are not sufficient to assess the kinetics, since also knowledge about the energy barrier along the reaction path is of crucial importance.

The evolution of the amorphous phase upon crystallization can best be described in terms of the ring statistics. As explained before, four-membered rings with ABAB-alternation, resembling the crystalline structure, are obtained in the amorphous phase. Hegedus and Elliott^[68] performed molecular dynamics simulations on $\text{Ge}_2\text{Sb}_2\text{Te}_5$, simulating a whole phase-change cycle, that is melt-quenching and subsequent re-crystallization. From this, the time-resolved evolution of wrong bonds and near-regular four-fold rings (i.e., near-planar, near-rectangular four-fold rings) was obtained. Indeed, crystallization leads to a decrease in the concentration of wrong bonds. Simultaneously, the concentration in the number of the near-regular four-fold rings increases. Thus, a concise model of the phase transition in $\text{Ge}_2\text{Sb}_2\text{Te}_5$ is obtained. The procedure might be applied to other materials to gain composition-dependent insight into the mechanism of crystallization.

4.3.3. Pressure-Induced Amorphization

An alternative route to amorphization of Ge:Sb:Te-based phase-change materials has been identified as the application of hydrostatic pressure. Though the necessary pressures are not immediately relevant for applications, respective measurements provide interesting information on the crystalline structure and the phase transition. For pressures up to about 10 GPa, the decrease of the splitting of Ge-Te bond lengths, that is the strength of atomic distortion, is observed, but the crystallinity is maintained.^[147] Kolobov et al.^[148] found by X-ray diffraction and absorption fine structure measurements that for the metastable crystalline phase of $\text{Ge}_2\text{Sb}_2\text{Te}_5$, the lattice periodicity ceased in the pressure interval between 10 and 20 GPa. A similar result was subsequently obtained for $\text{Ge}_1\text{Sb}_2\text{Te}_4$.^[149] However, the amorphization pressure is smaller, which is correlated to the fact that the concentration of intrinsic vacancies is higher in $\text{Ge}_1\text{Sb}_2\text{Te}_4$ (12.5%) than in $\text{Ge}_2\text{Sb}_2\text{Te}_5$ (10%). It has been argued, that these vacancies are crucial for the amorphization of crystalline Ge:Sb:Te-materials. In favor of this explanation is the fact that pressure-induced amorphization is only obtained for the metastable crystalline phase in which intrinsic vacancies are randomly distributed. The stable crystalline phase does not show this effect.

Further investigation of the temperature-dependence by Krbal et al.^[150] does not show an influence up to 145 °C. The amorphization is irreversible upon decompression below 110 °C. The transition from the metastable to the stable phase upon annealing is hindered by pressures exceeding 5 GPa. Thus, it becomes clear that pressure-induced amorphization depends on the initial structure and that pressure affects the atomic

diffusivity that is necessary for the transition to the stable phase. This is underlined by the study of Krbal et al.^[151] Here, both the stable and the metastable phase have been exposed to high pressures. The metastable phase exhibited amorphization and crystallized again to a bcc-phase above 33 GPa. The stable phase, however, exhibited first a transition to an orthorhombic GeS-type structure and then also to a bcc phase. Both bcc-phases, however, are different. For instance only the bcc-phase formed from the stable phase reverted to the initial phase upon decompression.

While the pressure-induced amorphization was initially argued to mainly involve switching of germanium to tetrahedral positions similar to the umbrella-flip model, a different explanation was proposed based on a molecular dynamics simulation of $\text{Ge}_2\text{Sb}_2\text{Te}_5$ under pressure. Caravati et al.^[152] found that while the fraction of tetrahedral germanium increases with pressure, the absolute value remains even smaller (<20%) than for the melt-quenched models presented in Section 2.4. The mechanism of amorphization was investigated and shown to indeed involve the presence of vacancies; Te-atoms move towards the vacant sites, giving rise to homopolar Ge/Sb bonds in squared rings rotated by 45° with respect to the crystal axis.

It should be noted that pressure-induced amorphization likely leads to differences in structure as compared to both as deposited and melt-quenched amorphous samples. For instance, at the transition, the density is larger than for an uncompressed crystalline sample, while typical amorphous samples have a smaller density.

4.4. Electrothermal Modeling of the Phase Transition

For practical purposes such as the design of phase-change devices using a previously selected material, detailed knowledge about the atomic structure is not required. Instead, it becomes important to assess the details of electrical and heat conduction for all logical states during operation. This way, the correct functionality of a cell as well as the parameters of operation are determined. Hence, the geometrical distribution of amorphous and crystalline regions and their conductivities before, during and after the transition need to be known. Moreover, the properties of the surrounding material, in particular the thermal properties, are essential to the design and performance of a phase-change device. Various groups have engaged in modeling the phase transition in devices, though, we will not go into detail here.^[79,104,153–157]

5. Applications and Outlook

In the last section, our aim is to give an overview over the various applications that employ phase-change materials and their future development.

5.1. Optical Storage

Presently, optical data storage devices represent the most common application of phase-change based recording. With the introduction of blue laser light and maximization of the

numerical aperture, the race for higher resolution and hence the development of this field may at first seem exhausted. Room for increasing storage capacity would be left only by increasing the number of data layers per disk. At present, a 100 GB disk employing three data layers marks the upper limit for such data storage devices, paving the way to the fourth generation of commercial optical phase-change based media.^[158] However, another way of increasing capacity has been found in the course of phase-change research, that is near-field recording. Here, an optical element is placed close to the surface of the medium, at a distance that is much smaller than the optical wavelength. This allows to employ evanescent waves to manipulate bits on the medium beyond the diffraction limit.^[159] The so-called super-RENS effect (super-resolution near-field structure) refers to the observation that structures smaller than the optical wavelength can be obtained by combining phase-change films with an additional thin layer in optical near-field range.^[160] In other words, the part of the optical system that needs to be located very close to the phase-change film to enable near-field recording is incorporated into the disk structure itself. The extra layer typically functions as a dynamic aperture, which should at the same time be small and highly transmittive (aperture-type Super-RENS). Materials successfully employed for these mask layers typically comprise materials related to phase-change materials such as antimony,^[160,161] Sb_2Te_3 ,^[162] and PbTe ^[163] or even phase-change materials themselves.^[164]

Phenomenologically, it is clear that the laser illumination—or more precisely its intensity profile—must cause an optical non-linear response in the mask layer. The effect of super-resolution may be achieved by various types of interaction between matter and light. No consensus on the exact origin of the super-RENS-effect using the aforementioned materials has been reached yet. Mostly, a predominantly thermal effect is considered. Laser irradiation leads to heating of the resolution-enhancing layer. Since the optical properties of the mask layer material are temperature-dependent (thermoreflectance) an aperture is created.^[165] If even melting occurs at the center of the laser spot (given sufficient laser power is provided), the locally confined change in optical properties is even more pronounced. As a mean to gain information on structure and temperature of the respective portion of the mask layer, Raman scattering has been suggested.^[166] Li et al.^[167] proposed thermal expansion and the consequent change in light transmission as a possible origin for super-resolution effect. Tominaga et al.^[168] argued that super-RENS might stem from a ferroelectric catastrophe in the mask materials. Other authors consider a predominance of electronic effects such as saturable absorption due to band filling by free carriers.^[164,169] Liu and Wei^[170] state that the optical non-linear absorption characteristics (here of AIST) lead to recording beyond the diffraction limit. Thus, given the variety of proposed explanations but also the potential benefit, the field of phase-change based near-field recording remains a potentially rewarding research area.

5.2. Electronic Storage

When phase-change materials were introduced in 1968 by Ovshinsky,^[1] electronic memories were among their first

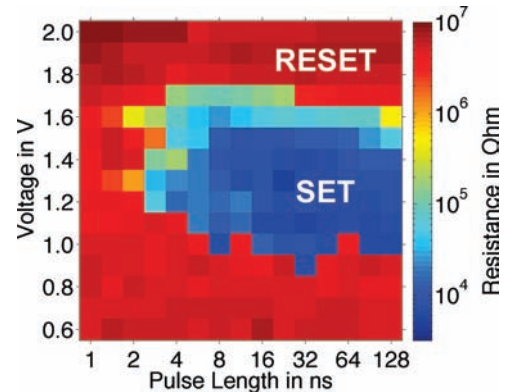


Figure 21. Characterization of a PCRAM-device employing GeTe as the active material using an electric tester. The visualization adopts the style of the corresponding power-time-effect diagrams from optical experiments using a static tester, cf. Figure 19. Here, crystallization, the time-limiting process involved in phase-change recording, can be triggered by applying pulses as short as only about 5 ns. Reproduced with permission from ref. [130]. Copyright 2009, American Institute of Physics.

suggested applications. Nevertheless, only now due to the availability of fast-switching phase-change materials and the ability to create nanoscaled structures, it is possible to create competitive, non-volatile phase-change based electronic memories: *phase-change random access memory*, usually abbreviated *PRAM* or *PCRAM*. As can be seen from the PTE-diagram shown in **Figure 21**, operation can proceed on the timescale of few nanoseconds which is orders of magnitude faster than Flash. This puts PCRAM in a position of a universal memory, that combines the best of both DRAM and Flash.^[97,171] Moreover, the attainable scalability even surpasses the existing memories, while having low power consumption. Hence, it is not surprising that the development of such memory cells has benefited from many industrial contributions.

Two principle designs of PCRAM cells have been proposed, line-cells and vertical structures, cf. **Figure 22**. A line-cell is simply a lateral line of a phase-change material that connects two electrodes. Given the large occupied area, its use is mainly limited to research projects—favoring the possibility to access the cell from the top—rather than actual memory devices. Though, some applications may exploit the ease of fabrication and low power consumption of these cells.^[97] The other type is a stack of layers, where a thin volume of phase-change is on top of a highly resistive heater element. Here, a portion of the phase-change volume that is close to the heater, that typically features a reduced diameter to increase the current density, is switched between the phases. Recently, an improved version of a PCRAM-cell has been realized that integrates the cell selector into the cell design.^[172] By the use of an Ovonic threshold-switch (OTS), a selector with no more than the same spatial footprint as the memory cell itself (i.e., $4F^2$, F being the feature size) is possible. This is to be contrasted with other, spatially more demanding designs mentioned in the recent review of Burr et al.^[107] The OTS is just a thin layer of a material that exhibits threshold-switching. If the voltage drop over the OTS due to the voltage applied between word- and bit line exceeds its threshold field, the memory cell, that is in series with the

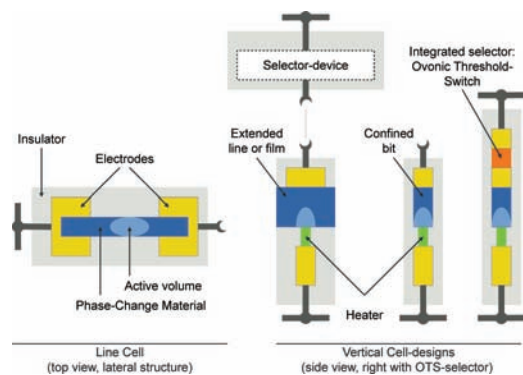


Figure 22. Comparison of typical designs of phase-change cells. While the lateral design is of particular interest to researchers, the vertical structures have a smaller lateral size and are thus favorable to achieve high storage densities. Here, one may distinguish between two sub-types with extended or confined volumes of a phase-change material. The former employ a thin layer (or line) of a phase-change material, while the latter involve pores in which the active volume more closely matches the actual volume of the material. Though this allows for a better control of the thermal environment of the cell, it also necessitates advanced production techniques that allow for high aspect ratios. Since the cells typically require also some selector devices, their actual spatial footprint is unfavorably enlarged. Thus, the concept shown on the very right is promising, where the selector is integrated into the cell design, not requiring any additional lateral space. It may consist of a material that exhibits threshold-switching and does not change its characteristics—for instance due to crystallization—throughout operation. Reproduced from ref. [2].

OTS, is selected. The simple design may also allow the stacking of layers of PCRAM-cells, increasing the storage density by making use of the third dimension.

PCRAM makes extensive use of the threshold switching effect presented in Section 3.2.3. In order to supply sufficient Joule heating power $P_j = U \cdot I = U^2/R(U)$ to quickly raise the temperature to levels high enough for crystallization to occur on a short timescale (cf. Figure 13), very high voltages would be required, if threshold switching would not occur. Thus, it allows to avoid voltage upconversion and the problems linked with high voltages in nanoscaled-electronics.

Production schemes for PCRAMs involve the development of techniques besides sputtering that allow for effective cell fabrication. For instance, large aspect ratios require techniques such as atomic layer deposition.^[173,174] So far, preparation techniques reported include chemical vapor deposition,^[175–179] evaporation,^[180,181] electrodeposition,^[182–184] pulsed laser deposition,^[185,186] and solution-phase deposition.^[187,188] Furthermore, selective etching of phase-change materials is investigated.^[189]

Among the criteria for a memory technique to be promising, scalability is a key requirement. It should be possible to exploit the steady improvement in reducing feature sizes in mass production to enable increasing data densities. Lack of scalability is one of the reasons why alternatives to Flash memory are actively pursued. Two factors may be discerned when scalability is addressed. On the one hand, the phase-change material must retain its properties despite reduction of its volume. On the other hand, the space taken up by dielectrics and the electronics necessary to address and control the memory cell must also be taken into account. Nano-scaling is particularly advantageous

to phase-change memory, since both energy consumption and crystallization time decrease with cell volume. The latter stems from the fact that with decreasing size of the memory cells, growth becomes the more prominent re-crystallization mechanism. The impact of nano-scaling on the material and device characteristics has recently been summarized in detail in the work of Raoux et al.^[108] Other aspects that we may subsume under scalability are the aforementioned prospect of stackability as well as multi-level storage via control of the amorphized volume fraction as introduced before.

So far, we have described the advantages of PCRAM over competing memory technologies in terms of its non-volatility, speed and attainable storage density. Another aspect, however, is cyclability (i.e., the number of possible write-cycles). The two main wear processes identified so far are electromigration and void formation. It is found that for cells based on Ge:Sb:Te-materials, the spatial distribution of the elements changes upon multiple set and reset operations. In particular, antimony accumulates at the cathode, pushing germanium aside. Thus, the composition in the active volume and thereby the cell properties change. Operation at reversed polarity, though, can “repair” such a cell.^[190] The density change upon crystallization and atomic mobility may also hamper the electrical contact via void formation.^[191] In addition, degradation of the electrodes (e.g., diffusion into the phase-change material) and phase segregation in the case of non-stoichiometric materials may also be regarded as limiting factors. Nevertheless, though the exact number of possible cycles depends on a variety of factors, it has been proven to exceed the corresponding value of Flash by several orders of magnitude.^[192]

5.3. Other Applications

Beyond the commercialized optical and electrical memories introduced before, a variety of possible future uses and research opportunities for phase-change materials have been investigated. The concept of probe-based storage envisions the use of an array of conductive AFM-tips to parallelly switch bits of a phase-change layer.^[155] It combines high resolution (i.e., storage density) with “simple” media. No costly production of the storage medium itself as it is the case for PCRAM is required. The interest in one-dimensional systems has been adopted by few phase-change researchers that have successfully synthesized and characterized phase-change nanowires for data storage.^[193–199]

Other authors seek to combine the reversible amorphous-to-crystalline transition with other material properties or device characteristics, that enable additional degrees of freedom to store or access data. Pandian et al.^[200,201] investigate the possibility of polarity-dependent resistance switching. By employing Sb-excess $\text{Ge}_2\text{Sb}_2\text{Te}_5$ in electrical cells, additional conductive Sb-filaments can be formed or broken. Thus, there is a second mechanism to set the resistivity of a cell. Song et al.^[202] incorporated iron into phase-change materials. This way, ferromagnetic, so-called *phase-change magnetic materials* could be obtained. For sufficiently small Fe-concentrations, it was possible to control the magnetization by switching between the phases. This observation was attributed to the difference in carrier concentration between both phases, since the carriers were

supposed to provide the required, indirect interaction between Fe-precipitates.

Finally, the fact that the resistivity of a phase-change cell depends on its history (i.e., more than just two logical states can be represented by one cell, that is multi-level storage becomes feasible) has led to the proposal of using such devices to emulate the behavior of synapses, paving the way for cognitive information processing.^[203] In that sense, phase-change based data storage does not only hold the potential to serve as a fast and reliable, universal non-volatile memory. Moreover, this technique could also revolutionize the way we process data.

Acknowledgements

The authors gratefully acknowledge financial support from the Deutsche Forschungsgemeinschaft (Wu 243/17). Furthermore, the authors would like to thank Matthieu Micoulaut as well as the members of the phase-change research group at RWTH Aachen University for fruitful discussions.

Received: November 18, 2010

Published online: April 5, 2011

- [1] S. R. Ovshinsky, *Phys. Rev. Lett.* **1968**, *21*, 1450.
- [2] D. Lencer, *Design Rules, Local Structure and Lattice-Dynamics of Phase-Change Materials for Data Storage Applications*, Doctoral thesis, RWTH Aachen University, **2010**.
- [3] N. Yamada, E. Ohno, N. Akahira, K. Nishiuchi, K. Nagata, M. Takao, *Jpn. J. Appl. Phys. Part 1* **1987**, *26*, 61.
- [4] N. Yamada, E. Ohno, K. Nishiuchi, N. Akahira, M. Takao, *J. Appl. Phys.* **1991**, *69*, 2849.
- [5] M. H. R. Lankhorst, L. van Pieterse, M. van Schijndel, B. A. J. Jacobs, J. C. N. Rijpers, *Jpn. J. Appl. Phys. Part 1* **2003**, *42*, 863.
- [6] J. Solis, C. N. Afonso, J. F. Trull, M. C. Morilla, *J. Appl. Phys.* **1994**, *75*, 7788.
- [7] L. van Pieterse, M. van Schijndel, J. C. N. Rijpers, M. Kaiser, *Appl. Phys. Lett.* **2003**, *83*, 1373.
- [8] C. Cabral, L. Krusin-Elbaum, J. Bruley, S. Raoux, V. Deline, A. Madan, T. Pinto, *Appl. Phys. Lett.* **2008**, *93*, 071906.
- [9] P. Zalden, C. Bichara, J. van Eijk, C. Braun, W. Bensch, M. Wuttig, *J. Appl. Phys.* **2010**, *107*, 104312.
- [10] M. N. Schneider, P. Urban, A. Leineweber, M. Doblinger, O. Oeckler, *Phys. Rev. B* **2010**, *81*, 184102.
- [11] W. Braun, R. Shayduk, T. Flissikowski, M. Ramsteiner, H. T. Grahn, H. Riechert, P. Fons, A. Kolobov, *Appl. Phys. Lett.* **2009**, *94*, 041902.
- [12] W. K. Njoroge, H. W. Woltgens, M. Wuttig, *J. Vacuum Sci. Technol. A* **2002**, *20*, 230.
- [13] T. P. L. Pedersen, J. Kalb, W. K. Njoroge, D. Wamwangi, M. Wuttig, F. Spaepen, *Appl. Phys. Lett.* **2001**, *79*, 3597.
- [14] J. Gonzalez-Hernandez, E. Prokhorov, Y. Vorobiev, *J. Vacuum Sci. Technol. A* **2000**, *18*, 1694.
- [15] E. Prokhorov, G. Trapaga, J. Gonzalez-Hernandez, *J. Appl. Phys.* **2008**, *104*, 103712.
- [16] J. L. F. Da Silva, A. Walsh, H. L. Lee, *Phys. Rev. B* **2008**, *78*, 224111.
- [17] J. P. Gaspard, A. Pellegatti, F. Marinelli, C. Bichara, *Phil. Mag. B* **1998**, *77*, 727.
- [18] P. B. Littlewood, *CRC Critical Rev. Solid State Mater. Sci.* **1984**, *11*, 229.
- [19] D. Lencer, M. Salinga, B. Grabowski, T. Hickel, J. Neugebauer, M. Wuttig, *Nat. Mater.* **2008**, *7*, 972.
- [20] K. Kifune, Y. Kubota, T. Matsunaga, N. Yamada, *Acta Crystallogr. Sect. B* **2005**, *61*, 492.
- [21] T. Matsunaga, H. Morita, R. Kojima, N. Yamada, K. Kifune, Y. Kubota, Y. Tabata, J. J. Kim, M. Kobata, E. Ikenaga, K. Kobayashi, *J. Appl. Phys.* **2008**, *103*, 093511.
- [22] Z. M. Sun, J. Zhou, R. Ahuja, *Phys. Rev. Lett.* **2006**, *96*, 055507.
- [23] Z. Sun, S. Kyrsta, D. Music, R. Ahuja, J. M. Schneider, *Solid State Commun.* **2007**, *143*, 240.
- [24] J. W. Park, S. H. Eom, H. Lee, J. L. F. Da Silva, Y. S. Kang, T. Y. Lee, Y. H. Khang, *Phys. Rev. B* **2009**, *80*, 115209.
- [25] B. J. Kooi, J. T. M. De Hosson, *J. Appl. Phys.* **2002**, *92*, 3584.
- [26] T. Matsunaga, N. Yamada, *Phys. Rev. B* **2004**, *69*, 104111.
- [27] M. Wuttig, D. Lusebrink, D. Wamwangi, W. Welnic, M. Gillissen, R. Dronskowski, *Nat. Mater.* **2007**, *6*, 122.
- [28] A. V. Kolobov, P. Fons, A. I. Frenkel, A. L. Ankudinov, J. Tominaga, T. Uruga, *Nat. Mater.* **2004**, *3*, 703.
- [29] S. Shamoto, N. Yamada, T. Matsunaga, T. Proffen, J. W. Richardson, J. H. Chung, T. Egami, *Appl. Phys. Lett.* **2005**, *86*, 081904.
- [30] U. V. Waghmare, N. A. Spaldin, H. C. Kandpal, R. Seshadri, *Phys. Rev. B* **2003**, *67*, 125111.
- [31] M. C. Jung, K. H. Kim, Y. M. Lee, J. H. Eom, J. Im, Y. G. Yoon, J. Ihm, S. A. Song, H. S. Jeong, H. J. Shin, *J. Appl. Phys.* **2008**, *104*, 074911.
- [32] J. Akola, R. O. Jones, *J. Phys. - Condensed Matter* **2008**, *20*, 465103.
- [33] S. Caravati, M. Bernasconi, T. D. Kuhne, M. Krack, M. Parrinello, *J. Phys. - Condensed Matter* **2009**, *21*, 255501.
- [34] J. J. Kim, K. Kobayashi, E. Ikenaga, M. Kobata, S. Ueda, T. Matsunaga, K. Kifune, R. Kojima, N. Yamada, *Phys. Rev. B* **2007**, *76*, 115124.
- [35] M. Wuttig, N. Yamada, *Nat. Mater.* **2007**, *6*, 824.
- [36] E. Garcia-Garcia, A. Mendoza-Galvan, Y. Vorobiev, E. Morales-Sanchez, J. Gonzalez-Hernandez, G. Martinez, B. S. Chao, *J. Vacuum Sci. Technol. A* **1999**, *17*, 1805.
- [37] B. S. Lee, J. R. Abelson, S. G. Bishop, D. H. Kang, B. K. Cheong, K. B. Kim, *J. Appl. Phys.* **2005**, *97*, 093509.
- [38] J. Orava, T. Wagner, J. Sik, J. Prikrýl, M. Frumar, L. Benes, *J. Appl. Phys.* **2008**, *104*, 043523.
- [39] W. Welnic, S. Botti, L. Reining, M. Wuttig, *Phys. Rev. Lett.* **2007**, *98*, 236403.
- [40] B. Huang, J. Robertson, *Phys. Rev. B* **2010**, *81*, 081204.
- [41] K. Shportko, S. Kremers, M. Woda, D. Lencer, J. Robertson, M. Wuttig, *Nat. Mater.* **2008**, *7*, 653.
- [42] M. B. Luo, M. Wuttig, *Adv. Mater.* **2004**, *16*, 439.
- [43] G. Lucovsky, R. M. White, *Phys. Rev. B* **1973**, *8*, 660.
- [44] D. G. Pettifor, *J. Phys.: C: Solid State Phys.* **1986**, *19*, 285.
- [45] C. Steimer, V. Coulet, W. Welnic, H. Dieker, R. Detemple, C. Bichara, B. Beuneu, J. P. Gaspard, M. Wuttig, *Adv. Mater.* **2008**, *20*, 4535.
- [46] M. Micoulaut, W. Welnic, M. Wuttig, *Phys. Rev. B* **2008**, *78*, 224209.
- [47] M. Micoulaut, R. Vuilleumier, C. Massobrio, *Phys. Rev. B* **2009**, *79*, 214205.
- [48] J. Y. Raty, V. V. Godlevsky, J. P. Gaspard, C. Bichara, M. Bionducci, R. Bellissent, R. Ceolin, J. R. Chelikowsky, P. Ghosez, *Phys. Rev. B* **2002**, *65*, 115205.
- [49] M. V. Coulet, D. Testemale, J. L. Hazemann, J. P. Gaspard, C. Bichara, *Phys. Rev. B* **2005**, *72*, 174209.
- [50] J. Y. Raty, V. Godlevsky, P. Ghosez, C. Bichara, J. P. Gaspard, J. R. Chelikowsky, *Phys. Rev. Lett.* **2000**, *85*, 1950.
- [51] C. Bichara, M. Johnson, J. Y. Raty, *Phys. Rev. Lett.* **2005**, *95*, 267801.
- [52] C. Bichara, M. Johnson, J. P. Gaspard, *Phys. Rev. B* **2007**, *75*, 060201.
- [53] J. Akola, R. O. Jones, *Appl. Phys. Lett.* **2009**, *94*, 251905.
- [54] S. Caravati, M. Bernasconi, M. Parrinello, *Phys. Rev. B* **2010**, *81*, 014201.
- [55] K. Hirota, K. Nagino, G. Ohbayashi, *J. Appl. Phys.* **1997**, *82*, 65.

- [56] S. Hosokawa, T. Ozaki, K. Hayashi, N. Happo, M. Fujiwara, K. Horii, P. Fons, A. V. Kolobov, J. Tominaga, *Appl. Phys. Lett.* **2007**, *90*, 131913.
- [57] K. S. Andrikopoulos, S. N. Yannopoulos, G. A. Voyiatzis, A. V. Kolobov, M. Ribes, J. Tominaga, *J. Phys. - Condensed Matter* **2006**, *18*, 965.
- [58] K. S. Andrikopoulos, S. N. Yannopoulos, A. V. Kolobov, P. Fons, J. Tominaga, *J. Phys. Chem. Solids* **2007**, *68*, 1074.
- [59] W. Welnic, A. Pamungkas, R. Detemple, C. Steimer, S. Blugel, M. Wuttig, *Nat. Mater.* **2006**, *5*, 56.
- [60] P. Jovari, I. Kaban, J. Steiner, B. Beuneu, A. Schops, A. Webb, *J. Phys. - Condensed Matter* **2007**, *19*, 335212.
- [61] P. Jovari, I. Kaban, J. Steiner, B. Beuneu, A. Schops, M. A. Webb, *Phys. Rev. B* **2008**, *77*, 035202.
- [62] S. Kohara, K. Kato, S. Kimura, H. Tanaka, T. Usuki, K. Suzuya, H. Tanaka, Y. Moritomo, T. Matsunaga, N. Yamada, Y. Tanaka, H. Suematsu, M. Takata, *Appl. Phys. Lett.* **2006**, *89*, 201910.
- [63] K. Kohary, V. M. Burlakov, D. G. Pettifor, *Phys. Rev. B* **2005**, *71*, 235309.
- [64] J. Akola, R. O. Jones, *Phys. Rev. B* **2007**, *76*, 235201.
- [65] J. Akola, R. O. Jones, *Phys. Rev. Lett.* **2008**, *100*, 205502.
- [66] J. Akola, R. O. Jones, *Phys. Rev. B* **2009**, *79*, 134118.
- [67] S. Caravati, M. Bernasconi, T. D. Kuhne, M. Krack, M. Parrinello, *Appl. Phys. Lett.* **2007**, *91*, 171906.
- [68] J. Hegedus, S. R. Elliott, *Nat. Mater.* **2008**, *7*, 399.
- [69] J. Akola, R. O. Jones, S. Kohara, S. Kimura, K. Kobayashi, M. Takata, T. Matsunaga, R. Kojima, N. Yamada, *Phys. Rev. B* **2009**, *80*, 020201.
- [70] M. Xu, Y. Q. Cheng, H. W. Sheng, E. Ma, *Phys. Rev. Lett.* **2009**, *103*, 195502.
- [71] G. C. Sosso, S. Caravati, M. Bernasconi, *J. Phys. - Condensed Matter* **2009**, *21*, 095410.
- [72] G. C. Sosso, S. Caravati, C. Gatti, S. Assoni, M. Bernasconi, *J. Phys. - Condensed Matter* **2009**, *21*, 245401.
- [73] T. Matsunaga, N. Yamada, *Jpn. J. Appl. Phys. Part 1* **2004**, *43*, 4704.
- [74] T. Matsunaga, N. Yamada, R. Kojima, S. Shamoto, M. Sato, H. Tanida, T. Uruga, S. Kohara, M. Takata, P. Zalden, G. Bruns, I. Sergueev, H. C. Wille, R. P. Hermann, M. Wuttig, *Adv. Funct. Mater.* **2011**, DOI: 10.1002/adfm.2011002274.
- [75] R. Mazzarello, S. Caravati, S. Angioletti-Uberti, M. Bernasconi, M. Parrinello, *Phys. Rev. Lett.* **2010**, *104*, 085503.
- [76] J.-S. Rhyee, K. H. Lee, S. M. Lee, E. Cho, S. I. Kim, E. Lee, Y. S. Kwon, J. H. Shim, G. Kotliar, *Nature* **2009**, *459*, 965.
- [77] H. K. Lyeo, D. G. Cahill, B. S. Lee, J. R. Abelson, M. H. Kwon, K. B. Kim, S. G. Bishop, B. K. Cheong, *Appl. Phys. Lett.* **2006**, *89*, 151904.
- [78] E. K. Kim, S. I. Kwon, S. M. Lee, H. Seo, J. G. Yoon, *Appl. Phys. Lett.* **2000**, *76*, 3864.
- [79] V. Giraud, J. Cluzel, V. Sousa, A. Jacquot, A. Dauscher, B. Lenoir, H. Scherrer, S. Romer, *J. Appl. Phys.* **2005**, *98*, 013520.
- [80] M. Kuwahara, O. Suzuki, N. Taketoshi, T. Yagi, P. Fons, J. Tominaga, T. Baba, *Jpn. J. Appl. Phys. Part 1* **2007**, *46*, 6863.
- [81] M. Kuwahara, O. Suzuki, Y. Yamakawa, N. Taketoshi, T. Yagi, P. Fons, T. Fukaya, J. Tominaga, T. Baba, *Jpn. J. Appl. Phys. Part 1* **2007**, *46*, 3909.
- [82] W. P. Risk, C. T. Rettner, S. Raoux, *Appl. Phys. Lett.* **2009**, *94*, 101906.
- [83] I. Friedrich, V. Weidenhof, W. Njoroge, P. Franz, M. Wuttig, *J. Appl. Phys.* **2000**, *87*, 4130.
- [84] J. Gonzalez-Hernandez, E. Lopezcruz, M. Yanezlimon, D. Strand, B. B. Chao, S. R. Ovshinsky, *Solid State Commun.* **1995**, *95*, 593.
- [85] D. Subramaniam, C. Pauly, M. Liebmann, M. Woda, P. Rausch, P. Merkelbach, M. Wuttig, M. Morgenstern, *Appl. Phys. Lett.* **2009**, *95*, 103110.
- [86] T. Siegrist, P. Jost, H. Volker, M. Woda, P. Merkelbach, C. Schlockermann, M. Wuttig, *Nat. Mater.* **2011**, *10*, 202.
- [87] A. H. Edwards, A. C. Pineda, P. A. Schultz, M. G. Martin, A. P. Thompson, H. P. Hjalmarson, C. J. Umrigar, *Phys. Rev. B* **2006**, *73*, 045210.
- [88] A. V. Kolobov, J. Tominaga, P. Fons, T. Uruga, *Appl. Phys. Lett.* **2003**, *82*, 382.
- [89] D. Adler, M. S. Shur, M. Silver, S. R. Ovshinsky, *J. Appl. Phys.* **1980**, *51*, 3289.
- [90] A. Pirovano, A. L. Lacaita, F. Pellizzer, S. A. Kostylev, A. Benvenuti, R. Bez, *IEEE Trans. Electron Devices* **2004**, *51*, 714.
- [91] S. Braga, A. Cabrini, G. Torelli, *Appl. Phys. Lett.* **2009**, *94*, 092112.
- [92] J. Robertson, K. Xiong, P. W. Peacock, *Thin Solid Films* **2007**, *515*, 7538.
- [93] J. K. Olson, H. Li, T. Ju, J. M. Viner, P. C. Taylor, *J. Appl. Phys.* **2006**, *99*, 103508.
- [94] S. A. Baily, D. Emin, *Phys. Rev. B* **2006**, *73*, 165211.
- [95] S. A. Baily, D. Emin, H. Li, *Solid State Communications* **2006**, *139*, 161.
- [96] D. Ielmini, Y. G. Zhang, *Appl. Phys. Lett.* **2007**, *90*, 192102.
- [97] M. H. R. Lankhorst, B. W. S. M. M. Ketelaars, R. A. M. Wolters, *Nat. Mater.* **2005**, *4*, 347.
- [98] D. Krebs, S. Raoux, C. T. Rettner, G. W. Burr, M. Salinga, M. Wuttig, *Appl. Phys. Lett.* **2009**, *95*, 082101.
- [99] D. Krebs, *Electrical Transport and Switching in Phase Change Materials*, Ph.D. thesis, RWTH Aachen University, **2010**.
- [100] D. Emin, *Phys. Rev. B* **2006**, *74*, 035206.
- [101] D. Ielmini, Y. G. Zhang, *J. Appl. Phys.* **2007**, *102*, 054517.
- [102] D. Ielmini, *Phys. Rev. B* **2008**, *78*, 035308.
- [103] A. Pirovano, A. L. Lacaita, A. Benvenuti, F. Pellizzer, R. Bez, *IEEE Trans. Electron Devices* **2004**, *51*, 452.
- [104] A. Redaelli, A. Pirovano, A. Benvenuti, A. L. Lacaita, *J. Appl. Phys.* **2008**, *103*, 111101.
- [105] K. Jandieri, O. Rubel, S. D. Baranovskii, A. Reznik, J. A. Rowlands, S. O. Kasap, *J. Mater. Sci.: Mater. Electron.* **2009**, *20*, 221.
- [106] V. G. Karpov, Y. A. Kryukov, S. D. Savransky, I. V. Karpov, *Appl. Phys. Lett.* **2007**, *90*, 123504.
- [107] G. W. Burr, M. J. Breitwisch, M. Franceschini, D. Garetto, K. Gopalakrishnan, B. Jackson, B. Kurdi, C. Lam, L. A. Lastras, A. Padilla, B. Rajendran, S. Raoux, R. S. Shenoy, *J. Vacuum Sci. Technol. B* **2010**, *28*, 223.
- [108] S. Raoux, W. Welnic, D. Ielmini, *Chem. Rev.* **2010**, *110*, 240.
- [109] M. Boniardi, A. Redaelli, A. Pirovano, I. Tortorelli, D. Ielmini, F. Pellizzer, *J. Appl. Phys.* **2009**, *105*, 084506.
- [110] I. V. Karpov, M. Mitra, D. Kau, G. Spadini, Y. A. Kryukov, V. G. Karpov, *J. Appl. Phys.* **2007**, *102*, 124503.
- [111] M. Mitra, Y. Jung, D. S. Gianola, R. Agarwal, *Appl. Phys. Lett.* **2010**, *96*, 222111.
- [112] D. Ielmini, D. Sharma, S. Lavizzari, A. L. Lacaita, *IEEE Trans. Electron Devices* **2009**, *56*, 1070.
- [113] C. A. Angell, K. L. Ngai, G. B. McKenna, P. F. McMillan, S. W. Martin, *J. Appl. Phys.* **2000**, *88*, 3113.
- [114] J. A. Kalb, M. Wuttig, F. Spaepen, *J. Mater. Res.* **2007**, *22*, 748.
- [115] J. Kalb, F. Spaepen, M. Wuttig, *J. Appl. Phys.* **2003**, *93*, 2389.
- [116] J. C. Phillips, *J. Non-Cryst. Solids* **1979**, *34*, 153.
- [117] P. Boolchand, D. G. Georgiev, B. Goodman, *J. Optoelectron. Adv. Mater.* **2001**, *3*, 703.
- [118] M. Micoulaut, *J. Phys.: Condens. Matter* **2010**, *22*, 285101.
- [119] P. Jovari, I. Kaban, W. Hoyer, R. G. Delaplane, A. Wannberg, *J. Phys. - Condens. Matter* **2005**, *17*, 1529.
- [120] D. A. Baker, M. A. Paesler, G. Lucovsky, S. C. Agarwal, P. C. Taylor, *Phys. Rev. Lett.* **2006**, *96*, 255501.
- [121] M. Micoulaut, J. Y. Raty, C. Otjacques, C. Bichara, *Phys. Rev. B* **2010**, *81*, 174206.

- [122] M. Belhadji, N. Benameur, J. M. Saiter, J. Grenet, *Phys. Status Solidi B-Basic Research* **1997**, *201*, 377.
- [123] M. H. R. Lankhorst, *J. Non-Cryst. Solids* **2002**, *297*, 210.
- [124] J. Bicerano, S. R. Ovshinsky, *J. Non-Cryst. Solids* **1985**, *74*, 75.
- [125] S. Raoux, M. Salinga, J. L. Jordan-Sweet, A. Kellock, *J. Appl. Phys.* **2007**, *101*, 044909.
- [126] T. Katsuyama, H. Matsumara, *J. Non-Cryst. Solids* **1992**, *139*, 177.
- [127] K. Kelton, A. L. Greer, *Nucleation in Condensed Matter: Applications in Materials and Biology*, Pergamon Materials Series, **2009**.
- [128] M. Salinga, *Phase Change Materials for Non-volatile Electronic Memories*, Ph.D. thesis, RWTH Aachen University, **2008**.
- [129] B. S. Lee, G. W. Burr, R. M. Shelby, S. Raoux, C. T. Rettner, S. N. Bogle, K. Darmawikarta, S. G. Bishop, J. R. Abelson, *Science* **2009**, *326*, 980.
- [130] G. Bruns, P. Merkelbach, C. Schlockermann, M. Salinga, M. Wuttig, T. D. Happ, J. B. Philipp, M. Kund, *Appl. Phys. Lett.* **2009**, *95*, 043108.
- [131] V. Weidenhof, I. Friedrich, S. Ziegler, M. Wuttig, *J. Appl. Phys.* **2001**, *89*, 3168.
- [132] B. J. Kooi, J. T. M. De Hosson, *J. Appl. Phys.* **2004**, *95*, 4714.
- [133] B. J. Kooi, W. M. G. Groot, J. T. M. De Hosson, *J. Appl. Phys.* **2004**, *95*, 924.
- [134] J. Kalb, F. Spaepen, M. Wuttig, *Appl. Phys. Lett.* **2004**, *84*, 5240.
- [135] J. A. Kalb, F. Spaepen, M. Wuttig, *J. Appl. Phys.* **2005**, *98*, 054910.
- [136] I. Friedrich, V. Weidenhof, S. Lenk, M. Wuttig, *Thin Solid Films* **2001**, *389*, 239.
- [137] V. Weidenhof, I. Friedrich, S. Ziegler, M. Wuttig, *J. Appl. Phys.* **1999**, *86*, 5879.
- [138] J. A. Kalb, C. Y. Wen, F. Spaepen, H. Dieker, M. Wuttig, *J. Appl. Phys.* **2005**, *98*, 054902.
- [139] N. Ohshima, *J. Appl. Phys.* **1996**, *79*, 8357.
- [140] B. J. Kooi, R. Pandian, J. T. M. De Hosson, A. Pauza, *J. Mater. Res.* **2005**, *20*, 1825.
- [141] S. Raoux, H. Y. Cheng, J. L. Jordan-Sweet, B. Munoz, M. Hitzbleck, *Appl. Phys. Lett.* **2009**, *94*, 183114.
- [142] P. K. Khulbe, E. M. Wright, M. Mansuripur, *J. Appl. Phys.* **2000**, *88*, 3926.
- [143] J. S. Wei, F. X. Gan, *Thin Solid Films* **2003**, *441*, 292.
- [144] M. Naito, M. Ishimaru, Y. Hirotsu, M. Takashima, *J. Appl. Phys.* **2004**, *95*, 8130.
- [145] G. F. Zhou, *Mater. Sci. Eng. A* **2001**, *304*, 73.
- [146] A. V. Kolobov, P. Fons, J. Tominaga, *Phys. Status Solidi B-basic Solid State Physics* **2009**, *246*, 1826.
- [147] P. Fons, A. V. Kolobov, J. Tominaga, Y. Katayama, *Nuclear Instruments & Methods In Phys. Research Section B-beam Interactions With Materials and Atoms* **2005**, *238*, 160.
- [148] A. V. Kolobov, J. Haines, A. Pradel, M. Ribes, P. Fons, J. Tominaga, Y. Katayama, T. Hammouda, T. Uruga, *Phys. Rev. Lett.* **2006**, *97*, 035701.
- [149] A. V. Kolobov, J. Haines, A. Pradel, M. Ribes, P. Fons, J. Tominaga, C. Steimer, G. Aquilanti, S. Pascarelli, *Appl. Phys. Lett.* **2007**, *91*, 021911.
- [150] M. Krbal, A. V. Kolobov, J. Haines, A. Pradel, M. Ribes, P. Fons, J. Tominaga, C. Levelut, R. Le Parc, M. Hanfland, *Appl. Phys. Lett.* **2008**, *93*, 031918.
- [151] M. Krbal, A. V. Kolobov, J. Haines, P. Fons, C. Levelut, R. Le Parc, M. Hanfland, J. Tominaga, A. Pradel, M. Ribes, *Phys. Rev. Lett.* **2009**, *103*, 115502.
- [152] S. Caravati, M. Bernasconi, T. D. Kuhne, M. Krack, M. Parrinello, *Phys. Rev. Lett.* **2009**, *102*, 205502.
- [153] K. B. Blyuss, P. Ashwin, A. P. Bassom, C. D. Wright, *Phys. Rev. E* **2005**, *72*, 011607.
- [154] Y. Zhang, J. Feng, H. Wang, B. C. Cai, B. Chen, *Jpn. J. Appl. Phys. Part 1* **2005**, *44*, 1687.
- [155] C. D. Wright, M. Armand, M. M. Aziz, *IEEE Trans. Nanotechnol.* **2006**, *5*, 50.
- [156] D. H. Kim, F. Merget, M. Forst, H. Kurz, *J. Appl. Phys.* **2007**, *101*, 064512.
- [157] C. D. Wright, K. Blyuss, P. Ashwin, *Appl. Phys. Lett.* **2007**, *90*, 063113.
- [158] N. Yamada, R. Kojima, T. Nishihara, A. Tsuchino, Y. Tomekawa, H. Kusada, in *European Phase-Change and Ovonic Symposium 2009*, **2009**.
- [159] E. Betzig, J. K. Trautman, *Science* **1992**, *257*, 189.
- [160] J. Tominaga, T. Nakano, N. Atoda, *Appl. Phys. Lett.* **1998**, *73*, 2078.
- [161] T. Fukaya, J. Tominaga, T. Nakano, N. Atoda, *Appl. Phys. Lett.* **1999**, *75*, 3114.
- [162] L. P. Shi, T. C. Chong, X. Hu, J. M. Li, X. S. Miao, *Jpn. J. Appl. Phys. Part 1* **2006**, *45*, 1385.
- [163] H. S. Lee, B. K. Cheong, T. S. Lee, K. S. Lee, W. M. Kim, J. W. Lee, S. H. Cho, J. Y. Huh, *Appl. Phys. Lett.* **2004**, *85*, 2782.
- [164] H. S. Lee, T. S. Lee, Y. Lee, J. Kim, S. Lee, J. Y. Huh, D. Kim, B. K. Cheong, *Appl. Phys. Lett.* **2008**, *93*, 221108.
- [165] M. Kuwahara, T. Shima, P. Fons, T. Fukaya, J. Tominaga, *J. Appl. Phys.* **2006**, *100*, 043106.
- [166] M. Kuwahara, T. Shima, P. Fons, J. Tominaga, *Appl. Phys. Expr.* **2009**, *2*, 082402.
- [167] J. M. Li, L. P. Shi, H. X. Yang, K. G. Lim, X. S. Miao, W. L. Tan, T. C. Chong, *Jpn. J. Appl. Phys. Part 1* **2007**, *46*, 4148.
- [168] J. Tominaga, T. Shima, M. Kuwahara, T. Fukaya, A. Kolobov, T. Nakano, *Nanotechnology* **2004**, *15*, 411.
- [169] H. S. Lee, B. K. Cheong, T. S. Lee, J. H. Jeong, S. Lee, W. M. Kim, D. Kim, *Jpn. J. Appl. Phys. Part 2* **2007**, *46*, L277.
- [170] J. Liu, J. S. Wei, *J. Appl. Phys.* **2009**, *106*, 083112.
- [171] M. Wuttig, *Nat. Mater.* **2005**, *4*, 265.
- [172] D. Kau, S. Tang, I. Karpov, R. Dodge, B. Klehn, J. Kalb, J. Strand, A. Diaz, N. Leung, J. Wu, S. Lee, T. Langtry, K. wei Chang, C. Papiagianni, J. Lee, J. Hirst, S. Erra, E. Flores, N. Righos, H. Castro, G. Spadini, in *Electron Devices Meeting (IEDM), 2009 IEEE International*, **2009**, 1–4.
- [173] J. Lee, S. Choi, C. Lee, Y. Kang, D. Kim, *Appl. Surf. Sci.* **2007**, *253*, 3969.
- [174] M. Ritala, V. Pore, T. Hatanpaa, M. Heikkila, M. Leskela, K. Mizohata, A. Schrott, S. Raoux, S. M. Rosnagel, *Microelectron. Eng.* **2009**, *86*, 1946.
- [175] A. Abrutis, V. Plausinaitiene, M. Skapas, C. Wiemer, O. Salicio, M. Longo, A. Pirovano, J. Siegel, W. Gawelda, S. Rushworth, C. Giesen, *Microelectron. Eng.* **2008**, *85*, 2338.
- [176] A. Abrutis, V. Plausinaitiene, M. Skapas, C. Wiemer, O. Salicio, A. Pirovano, E. Varesi, S. Rushworth, W. Gawelda, J. Siegel, *Chem. Mater.* **2008**, *20*, 3557.
- [177] B. J. Choi, S. Choi, Y. C. Shin, C. S. Hwang, J. W. Lee, J. Jeong, Y. J. Kim, S. Y. Hwang, S. K. Hong, *J. Electrochem. Soc.* **2007**, *154*, H318.
- [178] R. Y. Kim, H. G. Kim, S. G. Yoon, *J. Electrochem. Soc.* **2008**, *155*, D137.
- [179] R. Y. Kim, H. G. Kim, S. G. Yoon, *Integrated Ferroelectrics* **2007**, *90*, 80.
- [180] J. Frayret, E. Barthelemy, S. Albert, C. Vigreux, A. Pradel, *Optoelectron. Adv. Mater. - Rapid Commun.* **2009**, *3*, 260.
- [181] T. Wagner, J. Orava, J. Prikrýl, T. Kohoutek, M. Bartos, M. Frumar, *Thin Solid Films* **2009**, *517*, 4694.
- [182] Q. Huang, A. J. Kellock, S. Raoux, *J. Electrochem. Soc.* **2008**, *155*, D104.
- [183] D. DelFrari, S. Diliberto, N. Stein, C. Boulanger, J. M. Lecuire, *Thin Solid Films* **2005**, *483*, 44.
- [184] G. Leimkuhler, I. Kerkamm, R. Reineke-Koch, *J. Electrochem. Soc.* **2002**, *149*, C474.

- [185] M. Pavlista, M. Hrdlicka, P. Nemeč, J. Prikryl, M. Frumar, *Appl. Phys. A* **2008**, 93, 617.
- [186] V. Nazabal, M. Cathelinaud, W. Shen, P. Nemeč, F. Charpentier, H. Lhermite, M. L. Anne, J. Capoulade, F. Grasset, A. Moreac, S. Inoue, M. Frumar, J. L. Adam, M. Lequime, C. Amra, *Appl. Opt.* **2008**, 47, C114.
- [187] D. J. Milliron, S. Raoux, R. Shelby, J. Jordan-Sweet, *Nat. Mater.* **2007**, 6, 352.
- [188] D. B. Mitzi, S. Raoux, A. G. Schrott, M. Copel, A. Kellock, J. Jordan-Sweet, *Chem. Mater.* **2006**, 18, 6278.
- [189] Y. Lin, M. H. Hong, G. X. Chen, C. S. Lim, L. S. Tan, Z. B. Wang, L. P. Shi, T. C. Chong, *J. Mater. Processing Technol.* **2007**, 192, 340.
- [190] S. Lee, J. h. Jeong, T. S. Lee, W. M. Kim, B. k. Cheong, *Electron Device Lett. IEEE* **2009**, 30, 448.
- [191] L. Krusin-Elbaum, J. C. Cabral, K. N. Chen, M. Copel, D. W. Abraham, K. B. Reuter, S. M. Rosnagel, J. Bruley, V. R. Deline, *Appl. Phys. Lett.* **2007**, 90, 141902.
- [192] D. Ahn, S. Cho, H. Horii, D. Im, I.-S. Kim, G. H. Oh, S. Park, M. Kang, S. Nam, C. Chung, *European Phase-Change and Ovonic Symposium 2010* **2010**, 87.
- [193] Y. Jung, S. H. Lee, D. K. Ko, R. Agarwal, *J. Am. Chem. Soc.* **2006**, 128, 14026.
- [194] S. Meister, H. L. Peng, K. McIlwrath, K. Jarausch, X. F. Zhang, Y. Cui, *Nano Lett.* **2006**, 6, 1514.
- [195] S. H. Lee, D. K. Ko, Y. Jung, R. Agarwal, *Appl. Phys. Lett.* **2006**, 89, 223116.
- [196] S. H. Lee, Y. Jung, R. Agarwal, *Nat. Nanotechnol.* **2007**, 2, 626.
- [197] X. H. Sun, B. Yu, M. Meyyappan, *Appl. Phys. Lett.* **2007**, 90, 183116.
- [198] S. H. Lee, Y. W. Jung, R. Agarwal, *Nano Lett.* **2008**, 8, 3303.
- [199] S. Meister, D. T. Schoen, M. A. Topinka, A. M. Minor, Y. Cui, *Nano Lett.* **2008**, 8, 4562.
- [200] R. Pandian, B. J. Kooi, G. Palasantzas, J. T. M. De Hosson, A. Pauza, *Adv. Mater.* **2007**, 19, 4431.
- [201] R. Pandian, B. J. Kooi, J. L. M. Oosthoek, P. Van Den Dool, G. Palasantzas, A. Pauza, *Appl. Phys. Lett.* **2009**, 95, 252109.
- [202] W. D. Song, L. P. Shi, X. S. Miao, C. T. Chong, *Adv. Mater.* **2008**, 20, 2394.
- [203] S. R. Ovshinsky, *Jpn. J. Appl. Phys. Part 1* **2004**, 43, 4695.